

# F-Bench: Rethinking Human Preference Evaluation Metrics for Benchmarking Face Generation, Customization, and Restoration

Lu Liu<sup>1\*</sup>, Huiyu Duan<sup>1\*</sup>, Qiang Hu<sup>1</sup>, Liu Yang<sup>1</sup>, Chunlei Cai<sup>2</sup>,  
Tianxiao Ye<sup>2</sup>, Huayu Liu<sup>1</sup>, Xiaoyun Zhang<sup>1</sup>, Guangtao Zhai<sup>1</sup>

<sup>1</sup>Shanghai Jiao Tong University, Shanghai, China <sup>2</sup>Bilibili Inc., China

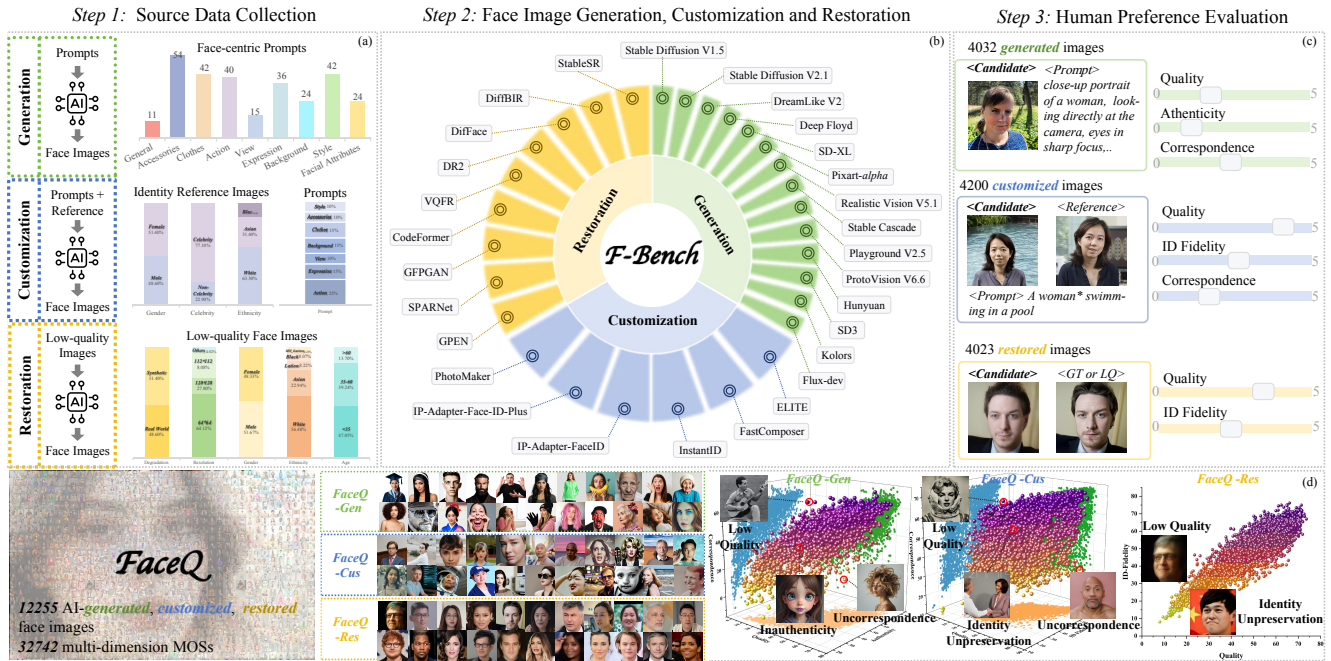


Figure 1. **Data construction pipeline of *F-bench* and content overview of *FaceQ* database.** (a) Diverse input source data for face generation, customization, and restoration. (b) *F-Bench* benchmarks 29 face generative models, including 14 face generation models, 6 face customization models, and 9 face restoration models. (c) Multi-dimensional subjective preference evaluation in *F-Bench*. (d) Visualization of the *FaceQ* database and 3D scatter plots of MOS distributions across three subsets.

## Abstract

Artificial intelligence generative models exhibit remarkable capabilities in content creation, particularly in face image generation, customization, and restoration. However, current AI-generated faces (AIGFs) often fall short of human preferences due to unique distortions, unrealistic details, and unexpected identity shifts, underscoring the need for a comprehensive quality evaluation framework for AIGFs. To address this need, we introduce **FaceQ**, a large-scale, com-

prehensive database of AI-generated **Face** images with fine-grained **Quality** annotations reflecting human preferences. The *FaceQ* database comprises 12,255 images generated by 29 models across three tasks: (1) face generation, (2) face customization, and (3) face restoration. It includes 32,742 mean opinion scores (MOSs) from 180 annotators, assessed across multiple dimensions: quality, authenticity, identity (ID) fidelity, and text-image correspondence. Using the *FaceQ* database, we establish **F-Bench**, a benchmark for comparing and evaluating face generation, customization, and restoration models, highlighting strengths and weaknesses across various prompts and evaluation dimensions. Additionally, we assess the performance of existing image

\* These authors contribute equally to this work.

quality assessment (IQA), face quality assessment (FQA), AI-generated content image quality assessment (AIGCIQA), and preference evaluation metrics, manifesting that these standard metrics are relatively ineffective in evaluating authenticity, ID fidelity, and text-image correspondence. The FaceQ database will be publicly available upon publication.

## 1. Introduction

Generative models, including VAE [34], GAN [17], and diffusion models [25, 66, 77], have achieved remarkable advancements in recent years. Numerous variants of these foundational models leverage generative priors for various face-related downstream tasks, such as face generation [63, 68, 71], face customization [44, 103], and face restoration [49, 84], producing creative, high-quality, and realistic face images.

However, despite these advancements, current AI-generated faces (AIGFs) still exhibit a range of perceptual flaws. Unlike natural face images, which may suffer from low-level degradations such as compression artifacts, noise, or blur, AIGFs often lack authenticity in human perception. For example, as shown in Fig.1, unique distortions in facial attributes, including AI-generated artifacts and misalignments, contribute to a notable bad face issue. Unrealistic details, such as over-glossy skin or disproportionate facial features, negatively impact user preference. Additionally, unexpected identity variations frequently arise in face customization and restoration tasks. These prevalent problems highlight the necessity of establishing a comprehensive quality evaluator for AIGFs.

Current face quality assessment databases [3, 7, 50, 79] are primarily based on real face images sourced from photographers or online collections, which differ significantly from AI-generated faces in terms of texture, structure, and artifact characteristics. While recent AIGC quality assessment efforts [35, 38, 46, 83, 96] have focused on general image quality, they pay little attention to the unique challenges posed by face images. Without an AIGF-specific database, existing quality assessment (QA) methods struggle to evaluate AI-generated faces accurately, often failing to address issues like authenticity and identity fidelity, which are central to the user’s perception of face images.

To address this gap, we propose **FaceQ**, a large-scale database for AI-generated faces, each meticulously annotated with fine-grained human preference scores. As illustrated in Fig.1, the FaceQ database contains 12,255 images generated by 29 generative models across three tasks: 1) face generation, 2) face customization, and 3) face restoration. For face generation and customization, diverse source content is collected, covering various categories of prompts and identities. For face restoration, both synthetic and real-

world degradations are included through a mixed, random degradation pipeline. In total, 32,742 mean opinion scores (MOSs) are obtained from 180 annotators across multiple evaluation dimensions, including quality, authenticity, identity (ID) fidelity, and text-image correspondence. Each dimension exhibits distinct distributions and characteristics.

Based on the proposed FaceQ database, we establish a subjective human preference benchmark, **F-Bench**, by comparing and evaluating current models for face generation, customization, and restoration. Model-wise advantages and disadvantages are thoroughly analyzed across various dimensions for all three tasks. In-depth class-wise comparisons provide a finer-grained evaluation of the models’ performance with respect to prompts and demographic factors. Additionally, we compare the performance of existing image quality assessment (IQA), face quality assessment (FQA), AI-generated content image quality assessment (AIGCIQA), and preference evaluation metrics on their correlation with human, demonstrating that these mainstream metrics perform relatively poor in evaluating the authenticity, identity fidelity, and text-to-image correspondence. Overall, our study provides valuable insights into current face generation, customization, and restoration models, offering guidance for the development of more accurate AIGF evaluators.

## 2. Related Work

### Face Generation & Customization & Restoration.

(1) For face generation models, earlier works such as GANs [17, 31, 81] have demonstrated significant influences. Recently, diffusion models [63, 68, 71] have achieved rapid developments in text-to-image generation. These models can be categorized into pixel-space diffusion models [11, 62, 64, 70], and latent space diffusion models [6, 45, 57, 59, 68]. (2) For face customization, this is a recently defined task that aims to create images of a specific person with the input of an identity reference image and prompts [95]. It can be divided into two categories including conventional test-time optimization [15, 37, 69] and tuning-free customization methods utilizing pre-trained diffusion models [10, 22, 44, 88, 97, 103]. (3) For face restoration, which aims to restore high-quality face images from their low-quality counterparts. Some traditional restoration methods utilize geometric priors [5, 9, 33] or reference priors [41, 42] while in recent years, exploring generative prior such as GAN priors [4, 20, 91, 102, 107] and diffusion priors [49, 84, 94, 104] has become a prevalent trend. Despite these improvements, the generated, customized, and restored images may suffer from various quality issues, highlighting the necessity of evaluators.

**Face Image Quality Assessment Database.** Existing face image quality assessment (FIQA) can be divided into Biometric FIQA [1] and Generic FIQA [3, 7, 56, 89].

Table 1. Comparison of **FaceQ** and existing AIGC quality assessment database (*top*) and face quality assessment databases (*bottom*). FaceQ is the first large AI-generated, customized and restored database with fine-grained multi-dimensional annotations.

Database	Domain	Source	Tasks	Images	Scores	Ratings	Dimensions
Pick-A-Pic ( <i>NeurIPS2023</i> ) [35]	General	AI-generated	1	500000	Pair	500000	Overall
HPS ( <i>ICCV2023</i> ) [96]	General	AI-generated	1	98807	Pair	98807	Overall
AGIQA-3K ( <i>TCSVT2024</i> ) [38]	General	AI-generated	1	2982	MOS	5964	Perception, Alignment
AGICIQA ( <i>CVPR2024</i> ) [83]	General	AI-generated	1	2400	MOS	7200	Quality, Authenticity, Correspondence
RichHF-18K ( <i>CVPR2024</i> ) [46]	General	AI-generated	1	17760	MOS	71040	Plausibility, Aesthetics, Text-image Alignment, Overall
PIQ23 ( <i>CVPR2023</i> ) [3]	Face	Real	1	5116	Pair	15348	Overall, Details, Exposure
CFIQA-20k ( <i>TMM2023</i> ) [79]	Face	Real	1	20000	MOS	20000	Overall
CGFIQA-40k ( <i>CVPR2024</i> ) [7]	Face	Real	1	39312	MOS	39312	Overall
FIQA ( <i>TPAMI2024</i> ) [50]	Face	Real	1	42125	MOS	42125	Overall
<b>FaceQ</b>	<b>Face</b>	<b>AI-generated, customized and restored</b>	<b>3</b>	<b>12255</b>	<b>MOS</b>	<b>32742</b>	<b>Quality, Authenticity, ID Fidelity, Correspondence</b>

BFIQA [1, 2, 23, 47, 56] methods are most developed to evaluate the biometric utility of facial components for robust face recognition, which may fail to get satisfying results in terms of perceptual quality [7]. Subsequently, GFIQA methods are designed to improve the face restoration performance and only prioritize the perceptual degradation in face images. Existing FIQA databases are listed in Tab. 1, which predominantly focus on real face images, while the problem of considering face quality in emerging AI-generated images remains unexplored.

**AIGC Quality Assessment Database.** In recent years, plenty of researchers have raised interest in assessing AI-generated images (AIGIs) quality [35, 38, 83, 96] by building various databases as shown in Tab 1. These databases can be categorized based on the type of annotation, which includes wide-range pair annotations [35, 96] and MOS annotations [38, 46, 83]. Single-dimensional pair-wise annotations [35] simplify the AIGI quality into an overall score, which may lead to inaccurate characterization compared to multi-dimensional annotations. All of these databases primarily focus on general AIGI images, leaving a notable gap in datasets dedicated to AI-generated face images.

### 3. FaceQ Database Construction

#### 3.1. Data Collection

##### 3.1.1. FaceQ-Gen Subset Collection

**Prompt Sources.** To generate face images, in *FaceQ-Gen* subset, we design 288 face-centric prompts categorized into nine types: *General*, *Accessories*, *Clothes*, *Action*, *View*, *Expression*, *Background*, *Style*, and *Facial Attributes*. The distribution can be seen in Fig. 1. In particular, for *Action* categories, we sample from MS-COCO [48] dataset. For other categories, 80 prompts are sourced from [44], while the remaining prompts are self-designed under the assistance of GPT-4o [18]. From the above scheme, we obtain 360 initial prompts as input. A filtering scheme is adopted to guarantee the prompts are face-centric, diverse, and ethical, resulting in 288 final prompts.

**Models Collection and Face Image Generation.** The

*FaceQ-Gen* subset comprises 14 recent and representative open-source face generation models, including Deep Floyd [11], Stable Diffusion V1.5 [67], Stable Diffusion V2.1 [67], SD-XL [59], Realistic Vision [65], Stable Cascade [58], ProtoVision V6.6 [60], SD3 [72], Playground V2.5 [39], Kolors [36], PixArt-alpha [6], Hunyuan [45], and Flux-dev [14]. Since our database focuses on the quality assessment of realistic human face images, each model’s negative prompt is configured to exclude “anime” and “semi-realistic” outputs by using terms like “worst quality”, “low quality”, “illustration”, “3D”, “2D”, “painting”, “cartoons”, “sketch”, “anime”, “animation”, “cartoon”, and “semi-realistic”. Safe sensors are enabled to filter out NSFW content. Ultimately, *FaceQ-Gen* includes a total of 4,032 generated facial images. To ensure diversity in quality, we reduce the sampling steps to one-fourth of each model’s default setting for 111 randomly selected prompts, with all generated images clearly labeled. Please refer to the *supplementary material* for additional configuration details.

##### 3.1.2. FaceQ-Cus Subset Collection

**Identity and Prompt Sources.** Face customization relies on a reference identity image and a guiding prompt. In *FaceQ-Cus*, the reference images consist of 35 unique identities. Among them, twenty-five identities are sourced from [44], while ten identities are collected by ourselves. The source prompts are selected and filtered from the *FaceQ-Gen* prompt list, as described in Sec. 3.1.1, with the exclusion of the *General* class, which may limit customization efficacy. In total, 20 prompts are chosen, and these are reformatted to meet the expected input requirements for different methods by substituting class words or trigger words as needed.

**Models Collection and Face Image Customization.** We select six representative identity-oriented image-to-image models for the *FaceQ-Cus* subset, including ELITE [95], FastComposer [97], IP-Adapter-FaceID [29], InstantID [88], IP-Adapter-Face-ID-Plus [28], and PhotoMaker V2 [44]. Specifically, ELITE [95] requires an additional subject mask, which is obtained using a pre-trained segmentation model [61]. PhotoMaker [44] supports both

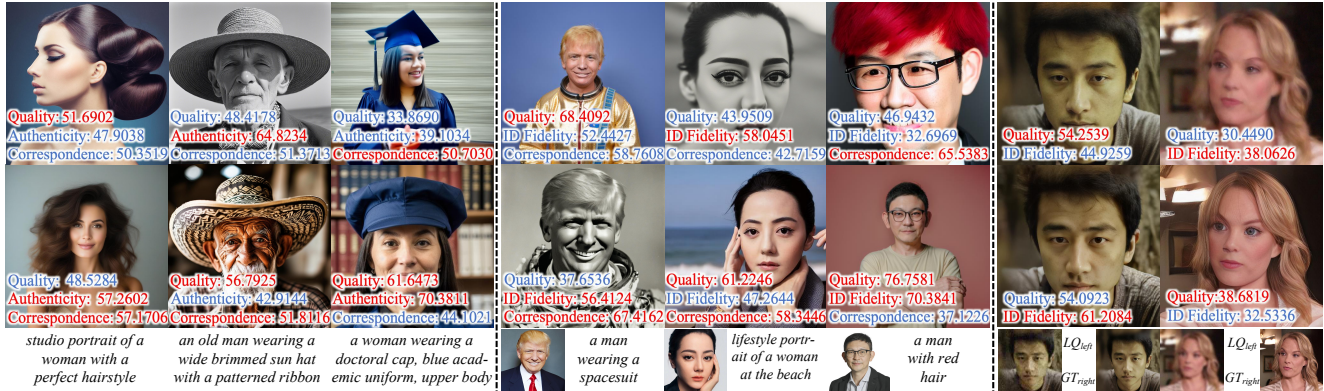


Figure 2. **Rating comparisons of eight dimensions.** Each column presents a pair of intuitive examples of each dimension, with red indicating the better rating and blue indicating the worse one. From left to right, the subsets are face generation, face customization, and face restoration subsets. The last row displays the corresponding prompts, reference image-prompt pairs, and the GT-LQ image pairs.

single and multiple reference images. For a fair comparison, we utilize only a single reference image. Universal negative prompt, NSWF filtering, and face-centric filtering are applied as described in Sec. 3.1.1. Finally, 700 images are generated per method, resulting in a total of 4,200 valid face images. Detailed configurations are provided in *supplementary material*.

### 3.1.3. FaceQ-Res Subset Collection

**Low Quality Images Source.** *FaceQ-Res* is divided into two categories based on the degradation type of low-quality images: synthetic and real-world. (1) **Synthetic:** To address the potential underrepresentation in previous works [43, 51], we additionally collect, crop, and align 100 high-quality Asian face images, each with a resolution of 512x512. In addition, we extract key frames from VFHQ [87] to avoid using the training set of restoration models. The data collection pipeline contains blur detection, occlusion detection, keyframe extraction, and keypoint alignment. Samples from the CelebRef dataset are also incorporated. To generate low-quality counterparts, we construct two degraded pipelines following previous works [4, 90, 92, 94] to simulate real-world degradations. In total, we obtain 224 HQ-LQ pairs. (2) **Real-world:** Real-world low-quality images consist of 223 low-quality images collected from various public datasets, including AgeAB [55], CelebChild [20], Wider [100], LFW [27] and MegaFace [32], ensuring the degradation diversity. Please refer to the *supplementary material* for more details.

**Models Collection and Face Image Restoration.** We evaluate several state-of-the-art methods, including diffusion-prior-based methods such as DiffBIR [49], DiffFace [104], StableSR [84], as well as GAN- and Transformer-based methods GFPGAN [91], GPEN [102], CodeFormer [107], VQFR [20] and Face-SPARNet [4]. We directly adopt their official code and pre-trained models. Each method is benchmarked on both the *F-Res* synthetic dataset and the real-

world dataset. In total, **4023** restored images are generated, with 2007 images in the real-world case and 2016 images in the synthetic case.

## 3.2. Human Preference Dimension Design

Traditional face quality assessments typically rely on a single evaluation dimension, which oversimplifies the evaluation process and fails to capture the unique strengths and weaknesses of different models, as well as individual user preferences. To address these limitations, we introduce a multi-dimensional approach that decomposes “face image quality” into four core dimensions: **Quality**, **Authenticity**, **ID Fidelity**, and **Correspondence**. These dimensions are further distributed across three categories—face generation, face customization, and face restoration—based on the specific characteristics of each task.

**Quality.** (*G-1, C-1, R-1*): This dimension evaluates the overall perceptual quality of the image, considering factors such as color accuracy, blur, noise, and artifacts. It is relevant to all three tasks (generation, customization, and restoration) and represents the visual fidelity of the image without considering text alignment or additional reference images.

**Authenticity.** (*G-2*): This dimension focuses on how closely the generated image resembles a natural, real-life photograph, with particular emphasis on realistic skin texture, facial details, and wrinkles. It is specifically used in face generation tasks, where ensuring a lifelike appearance is crucial.

**ID Fidelity.** (*C-2, R-2*): This dimension assesses how well the identity of the reference image is preserved in the generated or restored image. It is especially important in face customization and restoration tasks, where maintaining the identity of the individual is paramount.

**Correspondence.** (*G-3, C-3*): This dimension evaluates the degree of semantic consistency between the generated or customized image and the provided textual prompt. It is

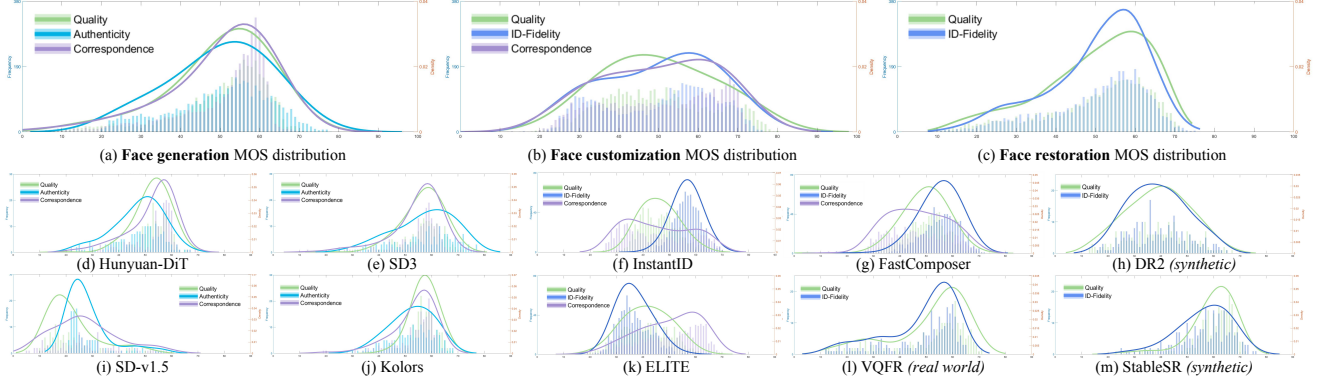


Figure 3. **Mean Opinion Score (MOS) distribution histograms and kernel density curves.** (a)-(c) MOS distributions for three subsets. (d)-(l) Model-wise MOS distributions. MOS Distributions of other methods are provided in the *supplementary material*.

relevant for both face generation and customization tasks, ensuring that the generated image aligns with the specified description.

### 3.3. Subjective Experiment

**Participants and Apparatus.** To ensure a comprehensive, fair, and reliable subjective assessment, 180 participants (90 female and 90 male) are recruited for the experiment, with 60 participants assigned to each task. All participants have normal or corrected-to-normal eyesight. Based on expert feedback, respective tutorials are designed for each task, and all participants complete the tutorial relevant to their assigned task. After the tutorial, participants are instructed to rate 20–30 practice images (10 per dimension) to ensure accurate assessments before proceeding to the main task. For the experimental apparatus, all images are displayed on 27-inch 4K Dell monitors, randomly presented, at their original resolution under standard lighting conditions. The experiment follows the ITU-R BT.500-14 guidelines [73] for subjective evaluations.

**Main Assessment.** We randomly divide 4032 generated images, 4200 edited images, and 4023 restored images into 12 groups, with each group containing approximately 1000 images from a specific task. The subjects are required to rate each image in a group by dragging a sliding window from 0 to 5 with a two-digit decimal on the following 2 or 3 dimensions. **(1) Face Generation:** *Quality* and *Authenticity* are single-stimulus dimensions; the text prompt only appears for the *Correspondence* dimension. **(2) Face Customization:** *Quality* and *Correspondence* are the same as face generation, while *ID Fidelity* is double-stimulus, with the ID reference image displayed only when adjusting the *ID Fidelity* slider. **(3) Face Restoration:** *Quality* is single-stimulus, while *Fidelity* is double- for real-world cases or multi-stimulus for synthetic cases.

**Subjective Score Post-processing.** For each group of ratings, outlier detection based on Kurtosis is conducted respectively with a rejection rate at 3% [73]. After removing

outliers, the valid raw ratings are converted and scaled into Z-scores ranging from  $[0, 100]$  with the following formulas:

$$z_{ij} = \frac{r_{ij} - \mu_j}{\sigma_j}, \quad z'_{ij} = \frac{100(z_{ij} + 3)}{6}, \quad (1)$$

$$\mu_j = \frac{1}{M_i} \sum_{i=1}^{M_i} r_{ij}, \quad \sigma_j = \sqrt{\frac{1}{M_i - 1} \sum_{i=1}^{M_i} (r_{ij} - \mu_j)^2}, \quad (2)$$

Here,  $r_{ij}$  represents the original ratings provided by the  $i$ -th evaluator for the  $j$ -th image,  $M_i$  denotes the total number of images that were assessed by the  $i$ -th participant in this group. Finally, the mean opinion score (MOS) of the image  $j$  ( $MOS_j$ ) is computed by averaging the rescaled z-scores as follows:

$$MOS_j = \frac{1}{N} \sum_{i=1}^N z'_{ij} \quad (3)$$

where  $N$  denotes the number of valid subjects, and  $z'_{ij}$  denotes rescaled z-scores.

Finally, a total of **491,130** reliable raw ratings are collected, with at least **15** valid ratings for each image. In total, **32,742** Mean Opinion Scores (MOS) are calculated across multiple dimensions.

## 4. F-Bench: Benchmarking Current Generative Face Models

### 4.1. Perspective Analysis

Fig. 3 (a)-(c) demonstrates the MOS distribution across eight dimensions in the three subsets, highlighting distinct variations between dimensions. (1) In the face generation task, the *Correspondence* score is the highest among the three dimensions, indicating that existing generative models perform well in aligning with prompts. The distribution of *Authenticity* is skewed towards lower scores, suggesting

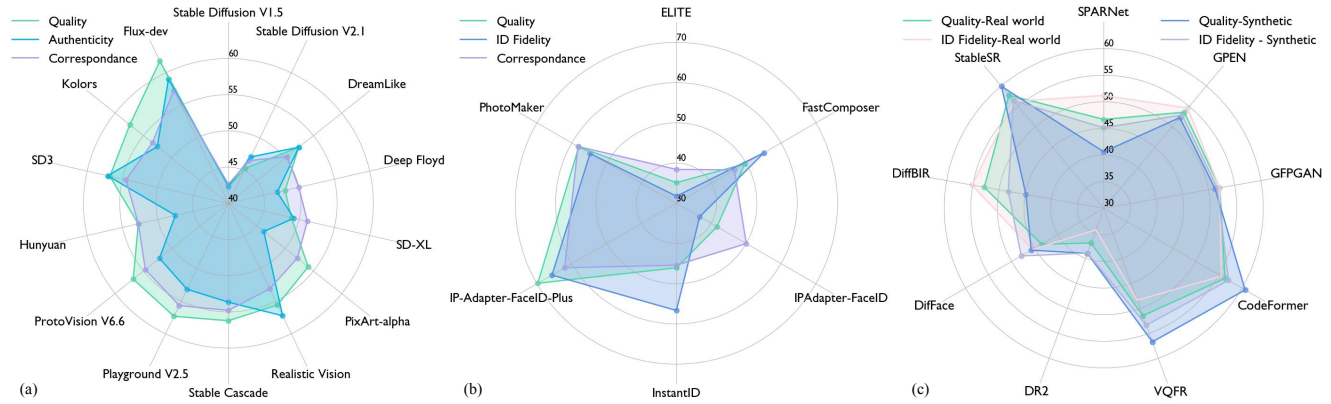


Figure 4. **Average MOS score comparison across all models and dimensions.** (a) Face generation. (b) Face customization. (c) Face restoration. The models are arranged in a clockwise order by release date.

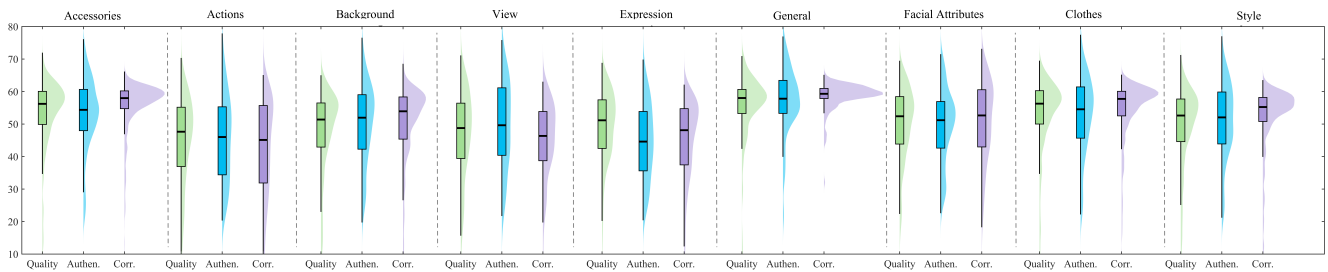


Figure 5. **Violin plots of quality, authenticity and correspondance scores in FaceQ-Gen subset across nine prompt categories.**

that current face generation models still fall short in generating photorealistic face images that satisfy human preferences. (2) In face customization, models perform the worst in the *Quality* dimension overall, demonstrating the difficulty of injecting identity information without compromising image quality. *Identity Fidelity* shows a bimodal distribution, reflecting the dichotomous nature of human judgment regarding whether the generated face accurately represents the same identity. (3) In face restoration, models perform better in *Quality* than in *Identity Fidelity*.

## 4.2. Model-wise Comparison

**Face Generation.** Fig. 16 (a) presents the average MOS scores across three dimensions: *Quality*, *Authenticity*, and *Correspondance*. *Correspondance* scores show a steady increase over time, indicating consistent improvement in text comprehension. *Quality* scores generally rise with the release year, although some methods, such as Hunyuan [45] and Dreamlike [13], exhibit deviations. Hunyuan [45] over-smoothes the facial details and performs worse compared to its contemporaries, while Dreamlike [13] performs the opposite. *Authenticity* scores exhibit the greatest variation among models, suggesting that current face generation models place insufficient emphasis on authenticity. Except for Realistic Vision [65], SD3 [72], Flux-dev [14], and Dreamlike [13], most models lag in authenticity relative to quality, highlighting a common phenomenon of high-quality but less realistic outputs in generative models. Fig. 3

(d, e, i, j) give four examples of MOS distributions of different methods, revealing a reasonable fine-grained performance difference. More examples and analyses can be seen in supplementary materials.

**Face Customization.** Fig. 16 (b) is the performance radar chart for face customization models. IP-Adapter-FaceID-Plus[28] achieves the best performance across all dimensions, followed by PhotoMaker [44]. This highlights their great robustness in identity encoders. ELITE [95] scores the lowest in all dimensions. IP-Adapter-FaceID [29] produces high-quality images but lacks accuracy in *Identity Fidelity*. This may be because the base model [59] introduces many AI artifacts, which affect both *Identity Fidelity* and *Quality*. InstantID [88] and FastComposer [97] score well in *Identity Fidelity* but underperform significantly in *Quality* and *Correspondance*, indicating strong identity preservation but limited text-driven editing capabilities. Fig. 3 (f, g, k) illustrate the model-wise MOS distributions, revealing similar trends to those observed in the radar chart.

**Face Restoration.** Fig. 16 (c) displays the average performance comparison of nine face restoration models. DR2 [94] exhibits the weakest performance in both *Quality* and *Identity fidelity*. This may be due to the degradation removal process of DR2 [94], which results in the loss of fine details and excessive smoothing. In contrast, StableSR [86] and CodeFormer [107] achieve the best overall performance among the nine face restoration models, successfully preserving both intricate details and accurate identity represen-

Table 2. **Performance benchmark on FaceQ-Gen and FaceQ-Cus subsets.** ♠, ♣, ♠, and ♡ denote traditional IQA models, face IQA models, classical deep learning-based IQA models, and AIGC IQA models respectively.

Task	Face Generation									Face Customization								
	Quality			Authenticity			Correspondence			Quality			Fidelity			Correspondence		
Model	SRCC↑	KRCC↑	PLCC↑	SRCC↑	KRCC↑	PLCC↑	SRCC↑	KRCC↑	PLCC↑	SRCC↑	KRCC↑	PLCC↑	SRCC↑	KRCC↑	PLCC↑	SRCC↑	KRCC↑	PLCC↑
♠NIQE [54]	0.1726	0.1142	0.2553	0.0869	0.0571	0.1346	0.0752	0.0507	0.1098	0.1365	0.0899	0.1436	0.1490	0.0991	0.1310	0.1186	0.0784	0.1245
♠ILNIQE [105]	0.1981	0.1319	0.3159	0.0675	0.0445	0.1505	0.0889	0.0591	0.1665	0.2032	0.1327	0.2479	0.2192	0.1452	0.2778	0.1878	0.1251	0.2275
♠HOSA [98]	0.2537	0.1708	0.2972	0.1103	0.0728	0.1446	0.122	0.0814	0.1495	0.1019	0.0688	0.0597	0.0753	0.0506	0.0552	0.1036	0.0696	0.0748
♠BPRI-PSS [52]	0.2362	0.1595	0.2413	0.1700	0.1142	0.1772	0.1673	0.1121	0.1647	0.0238	0.0166	0.0314	0.1425	0.0972	0.1758	0.1100	0.0729	0.1067
♠FISBLIM [19]	0.0901	0.0595	0.0433	0.0028	0.0003	0.0175	0.1000	0.0665	0.0196	0.1614	0.1024	0.1690	0.0256	0.0173	0.0126	0.0852	0.0559	0.0854
♣ArcFace[12]	N/A	N/A	N/A	N/A	N/A	N/A	N/A	N/A	N/A	0.3099	0.2094	0.3605	0.5062	0.3439	0.5572	0.1837	0.1243	0.2244
♣SER-FIQ[80]	0.1552	0.1034	0.1561	0.0470	0.0314	0.0575	0.1130	0.075	0.1110	-0.1241	-0.080	-0.1241	-0.0109	-0.0078	0.0042	-0.1680	-0.1121	-0.1911
♣DSL-FIQA[8]	0.5606	0.3927	0.5945	0.3156	0.2096	0.3960	0.3706	0.2514	0.4355	0.3615	0.2450	0.3651	0.2429	0.1652	0.2519	0.1040	0.0703	0.0974
♠CNNIQA [30]	0.4219	0.2895	0.3510	0.3037	0.2054	0.2973	0.2824	0.1931	0.2595	0.6244	0.4376	0.6620	0.6511	0.4441	0.6381	0.3765	0.2545	0.3264
♠VGG16 [76]	0.5846	0.4141	0.6006	0.5010	0.3508	0.5181	0.4349	0.2994	0.4723	0.7217	0.5324	0.7857	0.6735	0.4717	0.6636	0.5635	0.3932	0.5589
♠VGG19 [76]	0.5728	0.4043	0.5644	0.4681	0.3248	0.4479	0.4171	0.2873	0.4754	0.7952	0.6031	0.8096	0.7544	0.5417	0.7555	0.6585	0.4742	0.6465
♠ResNet18 [21]	0.6150	0.4417	0.6660	0.4600	0.3160	0.4604	0.4829	0.3360	0.4628	0.7966	0.6013	0.8006	0.7473	0.5335	0.7656	0.6308	0.4488	0.6191
♠ResNet34 [21]	0.6092	0.4354	0.6537	0.5564	0.3949	0.5401	0.4410	0.3065	0.5207	0.8141	0.6211	0.8151	0.7969	0.5878	0.8157	0.5708	0.4000	0.5810
♠HyperIQA [78]	0.6333	0.4545	0.6591	0.6106	0.4406	0.6042	0.4235	0.2912	0.4240	0.8524	0.6631	0.8205	0.8419	0.6463	0.8588	0.6628	0.4757	0.6454
♠TReS [16]	0.7766	0.5867	0.8047	0.6458	0.4703	0.6579	0.5708	0.4038	0.6270	0.8883	0.7083	<b>0.8951</b>	0.8330	0.6409	0.8658	0.7393	0.5497	0.7400
♠MANIQA [101]	<b>0.7871</b>	<b>0.5951</b>	<b>0.8150</b>	<b>0.7308</b>	<b>0.5436</b>	<b>0.7794</b>	<b>0.6278</b>	<b>0.4443</b>	<b>0.7066</b>	<b>0.8970</b>	<b>0.7185</b>	<b>0.8952</b>	<b>0.8590</b>	<b>0.6654</b>	<b>0.8796</b>	<b>0.7849</b>	<b>0.5941</b>	<b>0.7822</b>
♡CLIPScore [24]	0.0967	0.0642	0.1315	0.0640	0.0408	0.0817	0.2396	0.1591	0.2733	0.3126	0.2106	0.3185	0.1816	0.1218	0.1811	0.7008	0.5098	0.6986
♡BLIPScore [40]	0.1306	0.0872	0.1929	0.0935	0.0613	0.1569	0.2051	0.1364	0.2963	0.3073	0.2063	0.3136	0.1213	0.0796	0.1266	0.6707	0.4797	0.6123
♡ImageReward [99]	0.3849	0.2631	0.4358	0.2606	0.1736	0.3181	0.5155	0.3542	0.5871	0.3232	0.2166	0.3196	0.1905	0.1270	0.1839	0.7714	0.5673	0.7740
♡MINTIQA [85]	<b>0.8312</b>	<b>0.6474</b>	<b>0.8974</b>	<b>0.8177</b>	<b>0.6306</b>	<b>0.8511</b>	<b>0.7908</b>	<b>0.5991</b>	<b>0.8667</b>	<b>0.8904</b>	<b>0.7092</b>	0.8816	<b>0.8524</b>	<b>0.6697</b>	<b>0.8755</b>	<b>0.8391</b>	<b>0.6413</b>	<b>0.8318</b>

tations. When comparing the performance on real-world and synthetic data, most methods struggle to achieve satisfactory results on complex real-world degradations, except for SAPRNet [4] and DiffBIR [49]. StableSR [86] and GFPGAN [91] show strong robustness, performing consistently well on both real-world and synthetic data.

### 4.3. Class-wise Comparison

For the face generation task, we analyze the Mean Opinion Score (MOS) distributions of *Quality*, *Authenticity*, and *Correspondence* across nine prompt categories, as shown in Fig. 5. The violin plots highlight distinct performance patterns across these categories. The *Action*, *Expression*, and *Facial Attributes* categories exhibit lower MOS values in all three dimensions, with notable variability. In the *Action* category, limited visibility of the face due to body movements affects the generation of fine facial details, resulting in reduced scores, especially in *Quality* and *Correspondence*. The *Expression* category poses challenges in maintaining spatial relationships and physical constraints, leading to distortion and artifacts in expressions with exaggerated facial movements, such as laughing or crying, thereby impacting both *Quality* and *Authenticity*. For *Facial Attributes*, generating images with precise attributes (e.g., specific eye color, hair style) is challenging, particularly when multiple attributes are specified, which lowers the scores. In contrast, the *General* and *Background* categories achieve the highest MOS scores across all dimensions, as simpler or less specific prompts are easier for the model to interpret accurately. The *Clothes* and *Accessories* categories also perform well, indicating that the model handles clothes and accessory prompts effectively. In summary, prompts with

specific or complex attribute requirements tend to result in lower and more variable MOS values, while more general prompts or those with simple descriptions achieve consistently high performance across all three dimensions.

## 5. Performance Analysis on Current Quality Assessment Methods

### 5.1. Dataset and Benchmark Models

We conduct comprehensive experiments on the proposed *FaceQ* database to evaluate the effectiveness of current quality assessment methods, as shown in Tab.2, Tab.3, and Tab.4. The evaluation metrics for the benchmark models are SRCC, KRCC, and PLCC, which assess the correlation between the objective scores predicted by the QA methods and the subjective MOS scores provided by humans. The benchmark models are categorized into four categories:

**Traditional IQA Models.** NR-IQA models include NIQE [54], ILNIQE [105], HOSA [98], BPRI-PSS [52], FISBLIM [19]. FR-IQA models include LPIPS [106], SSIM [93] and PSNR [26].

**Classical Deep learning-based IQA Models.** This category includes CNNIQA [30], VGG16 [76], VGG19 [76], ResNet18 [21], ResNet34 [21], HyperIQA [78], TReS [16], MANIQA [101]. All models are retrained on our proposed database with an 80:20 training/testing split.

**AIGC IQA Models.** This category consists of pre-trained vision-language models, including CLIPScore [24], BLIP-Score [40], zero-shot metric ImageReward [99], and the AIGC-specific QA model MINTIQA [85].

**Face IQA Models.** This category includes SER-FIQ [80], DSL-FIQA [8] and pre-trained identity encoders ArcFace

Table 3. Performance benchmark on *FaceQ-Res* synthetic subset. ♠, ♡, ♣, and ◇ denote traditional NR-IQA models, FR-IQA models, face IQA models, and classical deep learning-based IQA models respectively.

Dimension Model	Quality			Authenticity		
	SRCC↑	KRCC↑	PLCC↑	SRCC↑	KRCC↑	PLCC↑
♠BMPRI[53]	0.2161	0.1428	0.1862	0.1113	0.0739	0.1069
♠NIQE[54]	0.1798	0.1213	0.1642	0.2193	0.1480	0.2118
♠ILNIQE[105]	0.2505	0.1727	0.3180	0.2696	0.1857	0.3321
♠HOSA[98]	0.3758	0.2522	0.3748	0.3418	0.3455	0.2301
♠BPRI-LSSn [52]	0.1398	0.0957	0.0999	0.1244	0.0837	0.0973
♠BPRI [52]	0.1637	0.1065	0.1480	0.0195	0.0121	0.0281
♠FISBLIM [19]	0.1589	0.1089	0.2038	0.1054	0.0709	0.1715
♡LPiPS[106]	0.3909	0.2658	0.4643	0.4372	0.3018	0.4870
♡SSIM[93]	0.1017	0.0675	0.0488	0.0933	0.0601	0.0504
♡PSNR [26]	0.0198	0.0113	0.0536	0.0986	0.0662	0.1212
♣ArcFace[12]	0.3466	0.2327	0.3774	0.5728	0.4030	0.5762
♣SER-FIQ [16]	0.3813	0.2584	0.3746	0.3951	0.2641	0.3707
♣DSL-FIQA [16]	0.6387	0.4508	0.6528	0.4882	0.3360	0.5379
◇CNNIQA [30]	0.4661	0.3197	0.3836	0.4678	0.3216	0.4288
◇ResNet18 [21]	0.7254	0.5295	0.6982	0.6662	0.4802	0.6527
◇ResNet34 [21]	0.6693	0.4916	0.6550	0.5905	0.4170	0.6084
◇VGG16 [76]	0.7487	0.5513	0.7101	0.6177	0.4413	0.6381
◇VGG19 [76]	0.6994	0.5126	0.6722	0.6038	0.4278	0.5999
◇HyperIQA [78]	0.8269	0.6323	0.8228	0.7615	0.5585	0.7471
◇MANIQA [101]	<b>0.8287</b>	<b>0.6403</b>	<b>0.8778</b>	<b>0.7704</b>	<b>0.5660</b>	<b>0.7619</b>
◇TReS [16]	<b>0.8656</b>	<b>0.6830</b>	<b>0.8622</b>	<b>0.7951</b>	<b>0.5879</b>	<b>0.7829</b>

Table 4. Performance benchmark on *FaceQ-Res* real-world subset. ♠, ♣, and ◇ denote traditional IQA models, face IQA models, and classical deep learning-based IQA models respectively.

Dimension Model	Quality			ID Fidelity		
	SRCC↑	KRCC↑	PLCC↑	SRCC↑	KRCC↑	PLCC↑
♠BMPRI[53]	0.1582	0.1093	0.2799	0.0149	0.0108	0.1386
♠NIQE[54]	0.1783	0.1186	0.1962	0.1245	0.0810	0.1701
♠ILNIQE[105]	0.2230	0.1610	0.2291	0.1964	0.1362	0.2340
♠HOSA[98]	0.3927	0.4277	0.2654	0.3328	0.2234	0.3813
♠BPRI-LSSn [52]	0.2715	0.1840	0.3022	0.2059	0.1380	0.2475
♠BPRI [52]	0.1920	0.1313	0.2200	0.0846	0.0570	0.1136
♠FISBLIM [19]	0.2512	0.1705	0.2725	0.2341	0.1581	0.2699
♣ArcFace[12]	0.2371	0.1565	0.4183	0.4956	0.3470	0.6330
♣SER-FIQ [16]	-0.0482	-0.0299	0.1023	0.0421	0.0299	0.1584
♣DSL-FIQA [16]	0.6509	0.4641	0.6494	0.4840	0.3362	0.5118
◇CNNIQA [30]	0.3650	0.2506	0.4705	0.3252	0.2197	0.3112
◇VGG16 [76]	0.4996	0.3439	0.4269	0.4117	0.2859	0.4622
◇VGG19 [76]	0.5871	0.4181	0.5133	0.3054	0.2044	0.3594
◇ResNet18 [21]	0.5977	0.4221	0.5722	0.5554	0.3909	0.6161
◇ResNet34 [21]	0.6259	0.4475	0.6168	0.5036	0.3539	0.6136
◇HyperIQA [78]	0.7926	0.5965	0.7926	<b>0.7783</b>	<b>0.5845</b>	<b>0.8163</b>
◇MANIQA [101]	<b>0.8356</b>	<b>0.6482</b>	<b>0.8467</b>	<b>0.7597</b>	<b>0.5655</b>	<b>0.8081</b>
◇TReS [16]	<b>0.8287</b>	<b>0.6391</b>	<b>0.8501</b>	0.7287	0.5441	0.8009

[12].

## 5.2. Performance Analysis

**Traditional IQA Models.** Traditional IQA methods, including both NR-IQA and FR-IQA models, generally perform poorly across all subsets and dimensions, with low SRCC, KRCC, and PLCC scores. These methods exhibit a significant discrepancy from human perception, particularly in quality and authenticity evaluation, likely due to

their limited ability to handle generative artifacts such as background blur.

**Classical Deep Learning-based IQA Models.** Deep learning-based IQA models, such as MANIQA [101] and HyperIQA [78], outperform traditional models with considerably higher correlation scores across dimensions. These models demonstrate enhanced sensitivity to image quality attributes relevant to human perception, achieving higher alignment with subjective ratings. However, they still encounter challenges with specific dimensions, especially when assessing complex attributes.

**AIGC IQA Models.** AIGC-focused models like MINTIQA [85] show competitive performance, especially in the quality and correspondence dimensions on generative tasks. MINTIQA [85] performs consistently well on synthetic and real-world subsets, suggesting it is better adapted to handle generative content. In contrast, CLIPScore [24] and BLIP-Score [40] show weaker correlations, likely due to their focus on high-level semantics rather than low-level details crucial for image quality assessment.

**Face IQA Models.** Face-specific IQA models (e.g., ArcFace [12], SER-FIQ [80], DSL-FIQA [8]) excel in evaluating ID fidelity, as seen in the real-world subset, where DSL-FIQA achieves high SRCC and PLCC scores. These models are optimized for identity consistency, making them particularly effective for tasks involving face quality and fidelity, though they may lack robustness in other general quality dimensions.

## 6. Conclusion

Evaluating the quality of AI-generated face images is a critical area of research in the development of generative models, given the human tendency to focus on faces. In this work, we introduce FaceQ, a meticulously curated AI face dataset comprising 12255 face images generated by 29 popular generative models, along with 32742 human annotated MOS scores. This dataset serves as a benchmark for evaluating the capabilities of existing face generation, customization, and restoration models, while also assessing the performance of current Image Quality Assessment (IQA) and Face Quality Assessment (FQA) methods. Our analysis highlights the unique features, strengths, and weaknesses of current face-related generative models, and reveals the limitations of traditional IQA and FQA algorithms in delivering subjectively consistent quality assessments for AI-generated faces. We believe FaceQ will contribute to advancing generative models and help overcome current limitations in face generation.

**Limitations and Social Impact.** Our evaluation framework has some limitations. First, we are mindful of privacy concerns related to face datasets, and all data collection and sharing adhere to relevant privacy policies. Second, while the maximum resolution in our dataset is limited



to 1024 pixels, we recognize that future work may incorporate higher-resolution images as generative models continue to advance. We hope that this work will contribute to improving the quality of AI-generated faces and foster the development of objective face evaluation metrics in generative modeling.

## A. FaceQ: Dataset Construction

### A.1. Face Generation, Customization and Restoration Models

**Model Implementation Details.** Tab. 5 provides a comprehensive summary of models evaluated for face generation, editing, and restoration, including the model links, released dates, the resolution, and the backbone architectures. (1) Face generation. All the generation models are inference by pre-trained checkpoints in their default resolutions and hyper-parameters. Specifically, Stable Diffusion V1.5 [68], DreamLike [13], and RealisticVision [65] support high-resolution generation, such as  $1024 \times 1024$ , but we utilize their default training resolution due to severe subject repetition phenomenon. Deep Floyd [11] is a 3-stage pixel space diffusion model, here we only consider the third-stage results. For the dynamic step sampling, the number of steps per stage for StableCascade [58] and Deep Floyd [11] is reduced to the quarter. (2) Face customization. All the customization models are inference by pre-trained checkpoints in their default resolutions and hyper-parameters. FastComposer [97], originally designed for multi-subject customization, is assessed here with a single reference image as input. We use the IP-Adapter release version, including IP-Adapter-FaceID-SDXL [29] and IP-Adapter-FaceID-PlusV2 [28] (referred to as IP-Adapter-FaceID and IP-Adapter-FaceID-Plus). Their backbones are SDXL and SD-v1.5, respectively. (3) Face restoration. For DR2 [94], we follow the hyperparameter settings recommended in the original paper:  $N = 4, T = 35$  for real-world inputs and  $N = 8, T = 35$  for synthetic inputs.

**Prompt Examples.** The face-centric prompts used for face generation can be categorized into nine classes. Tab. 6 presents two example prompts for each category due to space constraints. We ensured equal numbers of prompts for male and female subjects. The prompts for face customization are a subset of those used for face generation.

**Degradation Scheme.** We construct two synthetic degradation pipelines to mimic real-world degradation. The first is first order pipeline following previous works [4, 92, 94] which can be expressed as

$$I_d = [(I \otimes k_\sigma) \downarrow_r + n_\delta] \text{JPEG}_q \quad (4)$$

High-quality images are degraded through a series of operations, including blurring, downsampling, additive Gaussian

Table 5. Summary of 29 face generation, customization and restoration models.

Category	Model	Year	Resol.	Backbone
Face Generation	Stable Diffusion V1.5 [68]	2022.04	512 <sup>2</sup>	Latent Diffusion
	Stable Diffusion V2.1 [68]	2022.12	1024 <sup>2</sup>	Latent Diffusion
	DreamLike V2.0 [13]	2023.01	768 <sup>2</sup>	Latent Diffusion
	Deep Floyd [11]	2023.04	1024 <sup>2</sup>	Pixel Diffusion
	SD-XL [59]	2023.06	1024 <sup>2</sup>	Latent Diffusion
	PixArt-alpha [6]	2023.11	1024 <sup>2</sup>	Latent Diffusion (DiT)
	Realistic Vision V5.1 [65]	2023.12	512 <sup>2</sup>	Latent Diffusion
	Stable Cascade [58]	2024.02	1024 <sup>2</sup>	Latent Diffusion
	Playground V2.5 [39]	2024.02	1024 <sup>2</sup>	Latent Diffusion
	ProtoVision V6.6 [60]	2024.03	1024 <sup>2</sup>	Latent Diffusion
	Hunyuan [45]	2024.05	1024 <sup>2</sup>	Latent Diffusion (DiT)
	SD3 [72]	2024.07	1024 <sup>2</sup>	Latent Diffusion (DiT)
	Kolors [36]	2024.07	1024 <sup>2</sup>	Latent Diffusion
	Flux-dev [14]	2024.08	1024 <sup>2</sup>	Latent Diffusion (DiT)
Face Customization	ELITE [95]	2023.02	512 <sup>2</sup>	Latent Diffusion
	FastComposer [97]	2023.05	512 <sup>2</sup>	Latent Diffusion
	IP-Adapter-FaceID [29]	2023.12	512 <sup>2</sup>	Latent Diffusion
	InstantID [88]	2023.12	512 <sup>2</sup>	Latent Diffusion
	IP-Adapter-FaceID-Plus [28]	2023.12	512 <sup>2</sup>	Latent Diffusion
	PhotoMaker [44]	2023.12	512 <sup>2</sup>	Latent Diffusion
	SPARNet [4]	2020.12	512 <sup>2</sup>	GAN
	GPEN [102]	2021.05	512 <sup>2</sup>	GAN
	GFPGAN [91]	2021.06	512 <sup>2</sup>	GAN
	CodeFormer [107]	2022.08	512 <sup>2</sup>	VQ
	VQFR [20]	2022.07	512 <sup>2</sup>	VQ
	DiffFace [104]	2022.12	512 <sup>2</sup>	Pixel Diffusion
	DR2 [94]	2023.05	512 <sup>2</sup>	Pixel Diffusion
	DiffBIR [49]	2023.08	512 <sup>2</sup>	Latent Diffusion
	StableSR [86]	2024.06	512 <sup>2</sup>	Latent Diffusion

Table 6. Several examples of prompts for nine categories.

Category	Prompt Examples
General	a photo of a woman
	a photo of a middle-eastern man
Clothing	a woman wearing a purple wizard outfit
	a man wearing a hoodie with green stripes
Accessory	a man with black hair styled in a top bun
	an old woman with a vintage hairpin
Action	a woman coding in front of a computer
	a man playing the violin
Expression	a man crying disappointedly, with tears flowing
	a woman looking shocked, mouth wide open
Background	a woman laughing on the lawn
	a young woman with a colorful umbrella stands near a crowd
View	a man wearing a doctoral cap, upper body, with the left side of the face facing the camera
	a man playing the guitar in the view of left side
Style	instagram photo, portrait photo of a man, perfect face, natural skin, hard shadows, film grain
	editorial portrait of a man posing dramatically, sharp lighting, fashion magazine style
Facial Attributes	a young girl with large round blue eyes, a flat nose bridge, and purple lipstick
	A man with narrow black eyes, a high nose bridge, a thick beard, and fair skin

noise, and JPEG compression, with respective probabilities of 70%, 100%, 20%, and 70%. The blur kernel is randomly selected from Gaussian, Average, Median, and Motion blur. The interpolation method is randomly selected from Nearest, Linear, Area, and Cubic interpolation. The downsampling scale factor is randomly chosen from 4, 8, or 16. The second is a second-order degradation pipeline from previous work [90].

$$x = \mathcal{D}^n(y) = (\mathcal{D}_n \circ \dots \circ \mathcal{D}_2 \circ \mathcal{D}_1)(y). \quad (5)$$

Blur, resizing, noise, and JPEG compression are conducted in several orders, along with a sinc filter to simulate common ringing and overshoot artifacts. We used these two pipelines to generate 50% and 50% of the synthetic low-quality images, respectively.

## A.2. Additional Examples of *FaceQ* Database

Figure 6, Figure 7, and Figure 8 present additional examples from the *FaceQ-Gen*, *FaceQ-Cus*, and *FaceQ-Res* subsets, respectively. Each row corresponds to a specific generative model, showcasing the extensive diversity of content covered by the *FaceQ* dataset.

## A.3. Quantitative Analysis of *FaceQ* Database

We selected four low-level features—brightness, contrast, colorfulness, and sharpness—to quantitatively assess the content diversity of the *FaceQ* database. Fig. 9 illustrates the kernel distribution curves for each selected feature across the three subsets. The results indicate that the images in each subset exhibit a wide range of contrast, colorfulness, and sharpness. However, the *FaceQ-Cus* subset demonstrates a narrower distribution in terms of brightness compared to the other subsets. We further calculate the relative range  $R_i^k$  and coverage uniformity  $U_i^k$  of the three subsets across these selected features. The relative range  $R_i^k$  is defined as:

$$R_i^k = \frac{\max(C_i^k) - \min(C_i^k)}{\max_k(C_i^k)}, \quad (6)$$

where  $C_i^k$  denotes the distribution of  $k_{\text{th}}$  dataset on  $i_{\text{th}}$  feature.  $\max_k(C_i^k)$  refers to the maximum value of  $i_{\text{th}}$  feature across all datasets. The coverage uniformity  $U_i^k$  is calculated as the entropy of the B-bin histogram of  $C_i^k$  for each subset, using the following formula:

$$U_i^k = - \sum_{b=1}^B p_b \log_B p_b, \quad (7)$$

where  $p_b$  denotes the normalized number in bin  $b$  at  $i_{\text{th}}$  feature for  $k_{\text{th}}$  dataset. Fig. 10 presents a quantitative comparison of uniformity and relative range. A higher coverage uniformity indicates a more uniform feature distribution within

the database, while a higher relative range reflects greater intra- and inter-dataset differences. It can be observed that all three subsets exhibit a diverse range and a uniform distribution across the four low-level features.

## B. *FaceQ*: Subjective Experiments

### B.1. Implementation Details

Fig. 11 presents screenshots of the user rating interfaces for the four tasks. In the generation task, as shown in Figure 11 (a), participants are asked to rate images on a scale of 0 to 5 based on *quality*, *authenticity*, and *correspondence*. Prompts are displayed beneath the candidate images, accompanied by translations into the participants' native languages. In the customization task, as shown in Fig. 11 (b), the reference image is displayed on the left, with prompts and translation shown below. In Fig. 11 (c), the candidate image appears on the left, while the corresponding low-quality reference image is on the right. In Figure 11 (d), both the low-quality image and the ground truth are displayed in synthetic scenarios. Each subset in *FaceQ* was randomly divided into four groups, each containing approximately 1,000 images. Participants were compensated \$14 for completing each group of experiments according to [75]. At last, 3% invalid data are removed and no subject is removed.

### B.2. Subjective Evaluation Examples

Fig. 12 provides a visual supplement to the 3D scatter plots described in the main submission. Fig. 12 (a) presents the 3D scatter plot for the *FaceQ-Gen* subset, showcasing five representative edge points. These images, ranked from top to bottom, correspond to overall good, low correspondence, low authenticity, low quality, and overall bad. As illustrated, the MOS scores effectively and intuitively capture the strengths and weaknesses of the images, accurately reflecting human preferences across different dimensions. Similarly, Fig. 12 (b) depicts the 3D scatter plot for the *FaceQ-Cus* subset, highlighting another set of five representative points. These images, ranked from top to bottom, correspond to overall good, low correspondence, low identity correspondence, low quality, and overall bad. The MOS score demonstrates a significant decline in dimensions where the image exhibits poor performance. This observation further substantiates the reliability and validity of human scoring in reflecting image quality across multiple dimensions.

## C. *F-Bench*: More Analysis

### C.1. MOS Distribution

Fig. 13 illustrates the MOS distributions of all fourteen face generation models across the dimensions of quality, authenticity, and correspondence, for both full-step and 1/4-step



Figure 6. *FaceQ-Gen* Examples.

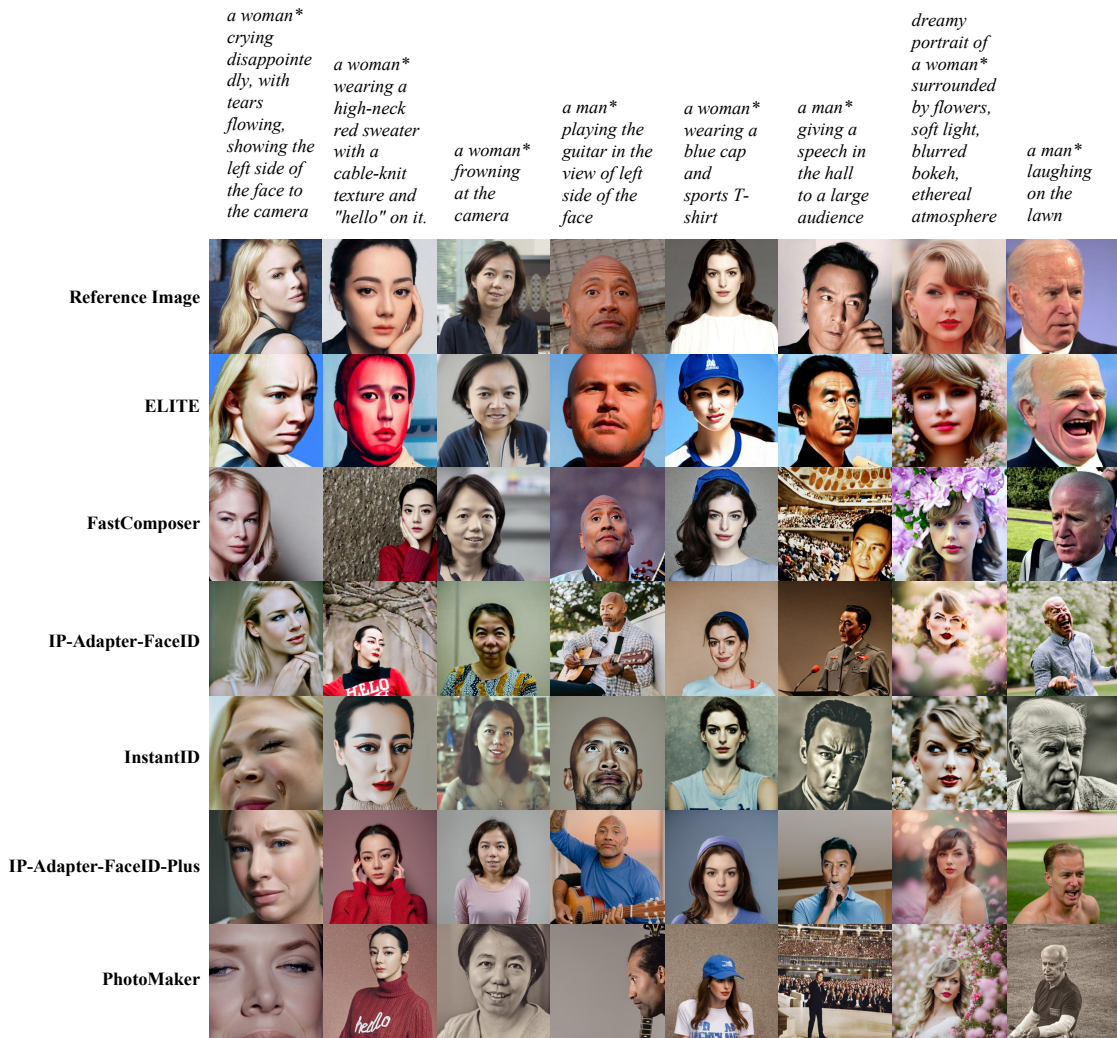


Figure 7. *FaceQ-Cus* Examples.

performances. The full-step distribution plots provide a comprehensive view of the performance distribution for different methods across the three dimensions, enabling a detailed evaluation of each method’s effectiveness. In the 1/4-step distribution plots, it can be observed that models such as Stable Cascade [58], SDXL [59], and Pixart-alpha [6] exhibit high sensitivity to the reduction in step size. In contrast, models such as Flux[14] and RealisticVision[65] demonstrate relatively stable performance with minimal degradation when reducing the steps. Fig. 14 illustrates the MOS distributions for six face customization models across three dimensions: quality, identity fidelity, and correspondence. Significant variations can be observed among different models and dimensions, highlighting distinct performance characteristics. Fig. 15 illustrates the MOS distributions for all nine face restoration models across the dimensions of quality and identity fidelity, evaluated for both real-world and synthetic cases. Most models exhibit varying performance between real-world and synthetic inputs,

resulting in noticeable differences in their distributions, as exemplified by SPARNet [4].

### C.2. Perspective Analysis

To provide a clearer comparison of the strengths and weaknesses of different methods, we present the average MOS scores across various dimensions in Figure 16. For the three dimensions of face generation, *authenticity* exhibits the largest disparity between methods, while *correspondence* and *quality* tend to cluster around higher scores. In the face customization task, the methods show inconsistent performance in *correspondence*, whereas *quality* remains relatively balanced. For face restoration, *quality-synthetic* emerges as the easiest metric to achieve high scores, followed by *quality-real-world*. Figure 17 displays the rankings of the various methods. For face generation, Flux [14] achieves the highest performance across all three dimensions. When considering *authenticity*, RealisticVision [65] and SD3 [72] outperform other methods. Playground [39]

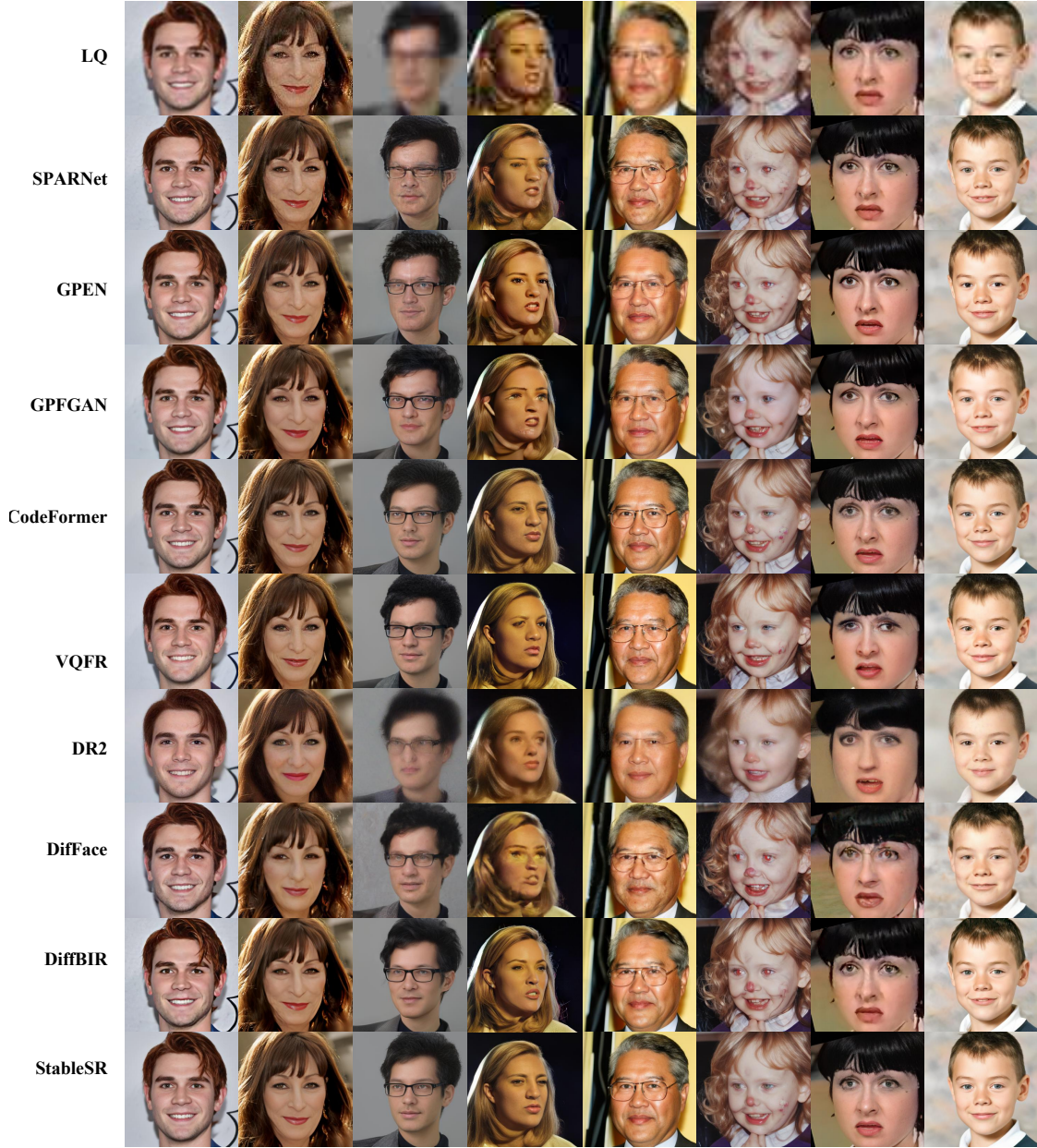


Figure 8. *FaceQ-Res* Examples.

ranks second only to Flux [14] in terms of *correspondence*, while Kolors [36] and SD3 [72] follow Flux [14] in *quality*. On the other hand, SDv1.5 [67] performs the worst across all dimensions. For face customization, IP-Adapter-FaceID-Plus [28], InstantID [88], and PhotoMaker [74] excel at preserving identity information. For face restoration, CodeFormer [107] demonstrates the best performance in synthetic scenarios, while StableSR achieves the highest scores in real-world scenarios.

### C.3. Class-wise Comparison

**Age.** Figure 18 presents the multi-dimensional MOS distributions across three age groups (Young, Middle-aged, and Old) for face generation, face customization, and face restoration tasks. In the face generation task, the performance across age groups is relatively consistent across all dimensions. For face customization, more pronounced differences are observed, particularly in the *quality* scores, where older individuals exhibit larger variability. In the face restoration task, *quality* scores for old individuals are no-

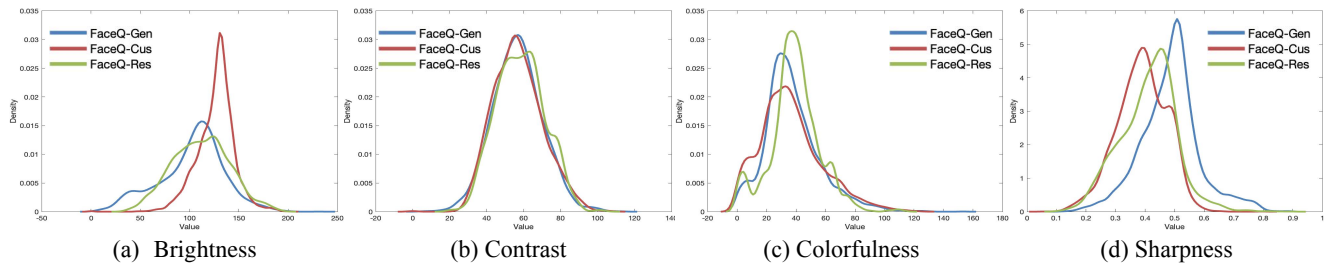


Figure 9. Comparisons of the selected four low-level feature distributions calculated on proposed *FaceQ* dataset.

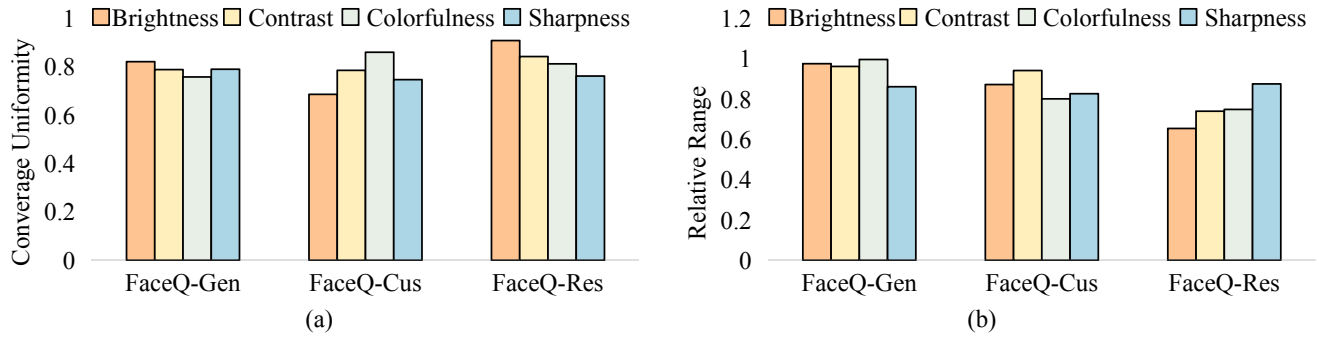


Figure 10. Comparisons of the selected four low-level features calculated on the proposed *FaceQ* dataset. (a) Coverage uniformity. (b) Relative range.

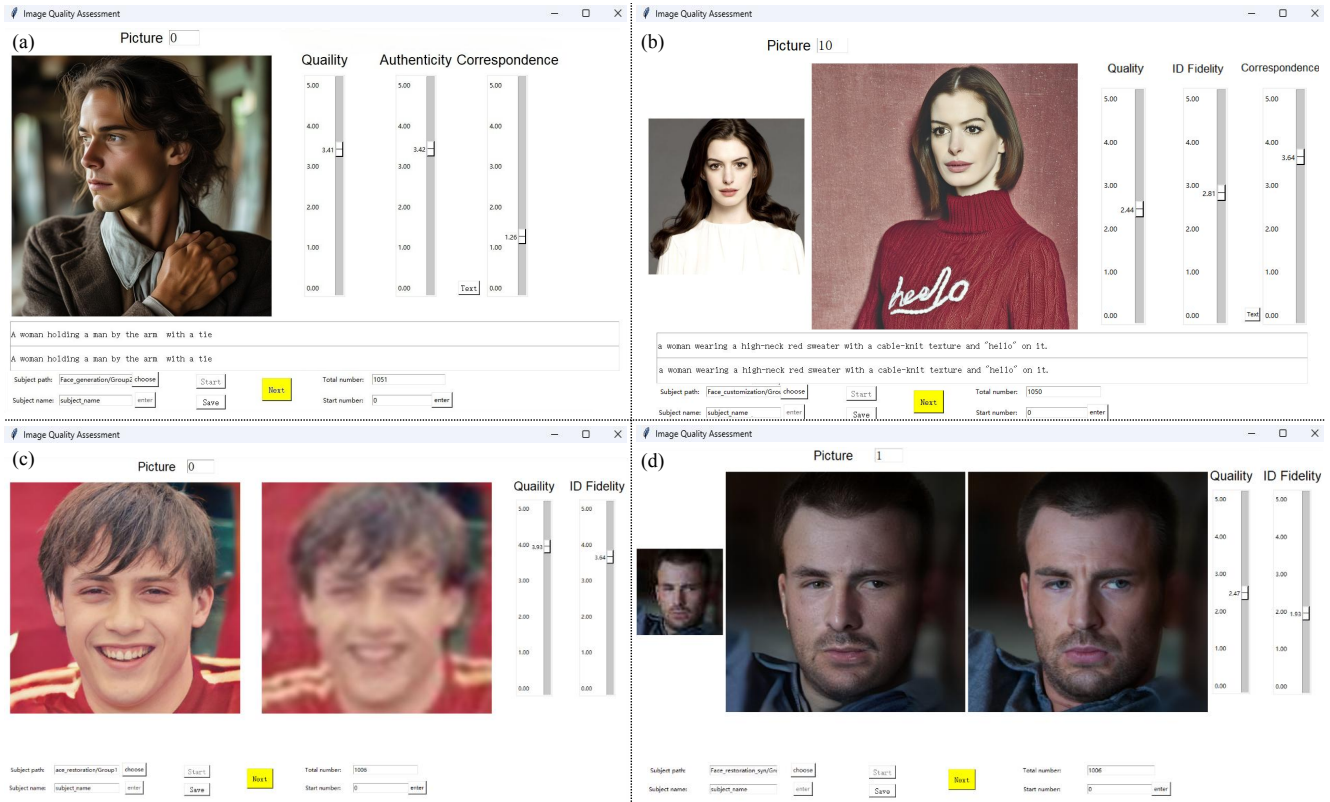


Figure 11. Screenshots of the rating interface for human evaluation. (a) Face generation evaluation interface. (b) Face customization evaluation interface. (c) Face restoration (real world) evaluation interface. (d) Face restoration (synthetic) evaluation interface.

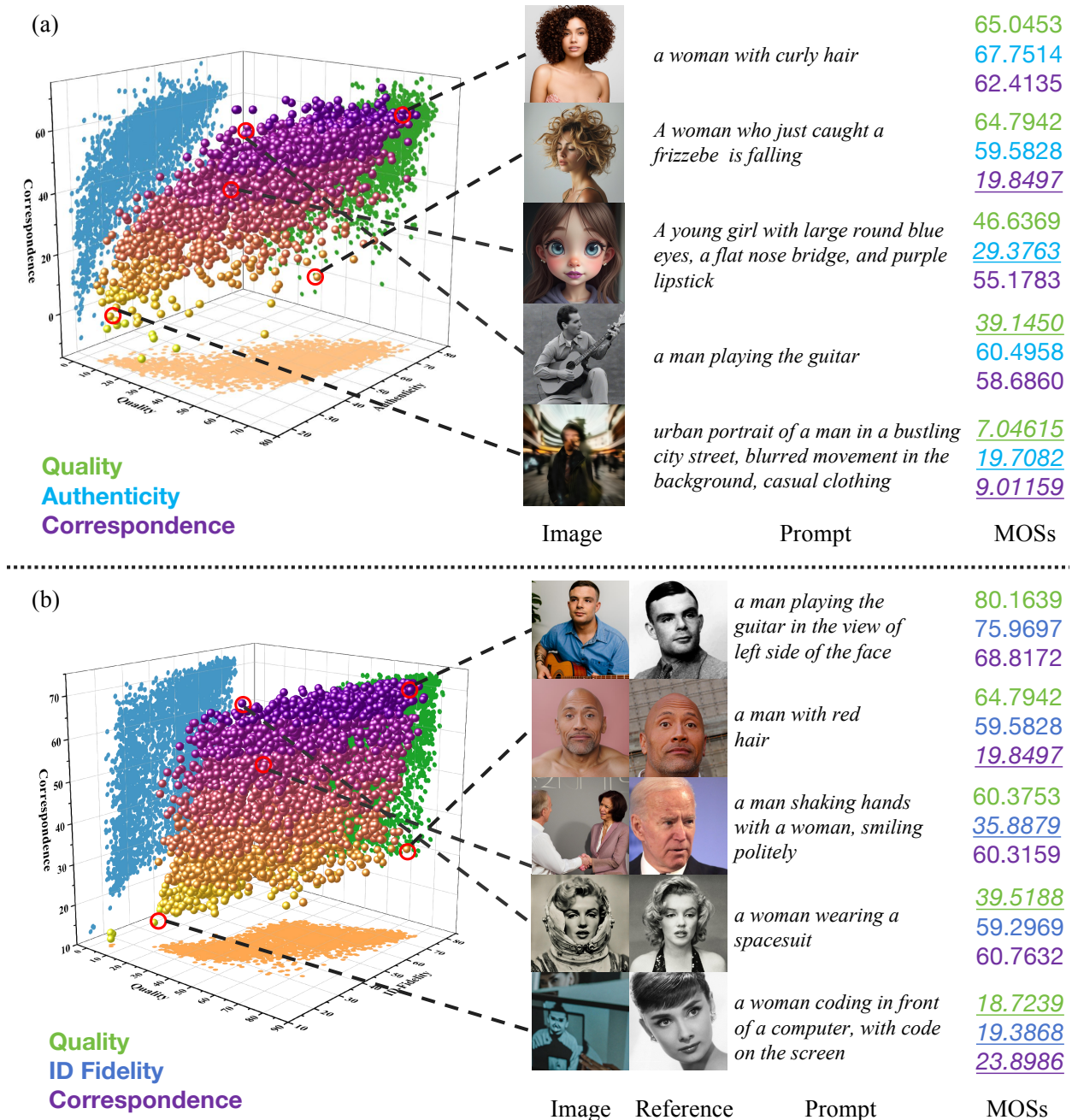


Figure 12. **Additional visualizations of the 3D scatter of MOSs.** We sample five representative points from the scatter and visualize their MOS scores across three dimensions. Each dimension is represented by a different color. The relatively low dimensions are underlined. (a) Face generation. (b) Face customization.

tably higher compared to middle-aged and young groups, while *identity fidelity* remains relatively consistent. These results highlight that face generation models are less sensitive to age-related factors, whereas face customization and restoration models demonstrate noticeable performance disparities among age groups, especially in dimensions such as

ID Fidelity and Quality. The age and gender of the images are labeled InsightFace.

**Gender.** We visualize the distribution of MOS scores in three dimensions for men and women in each dimension in Fig. 19. It can be found that the male and female categories in face generation and face customization perform consis-

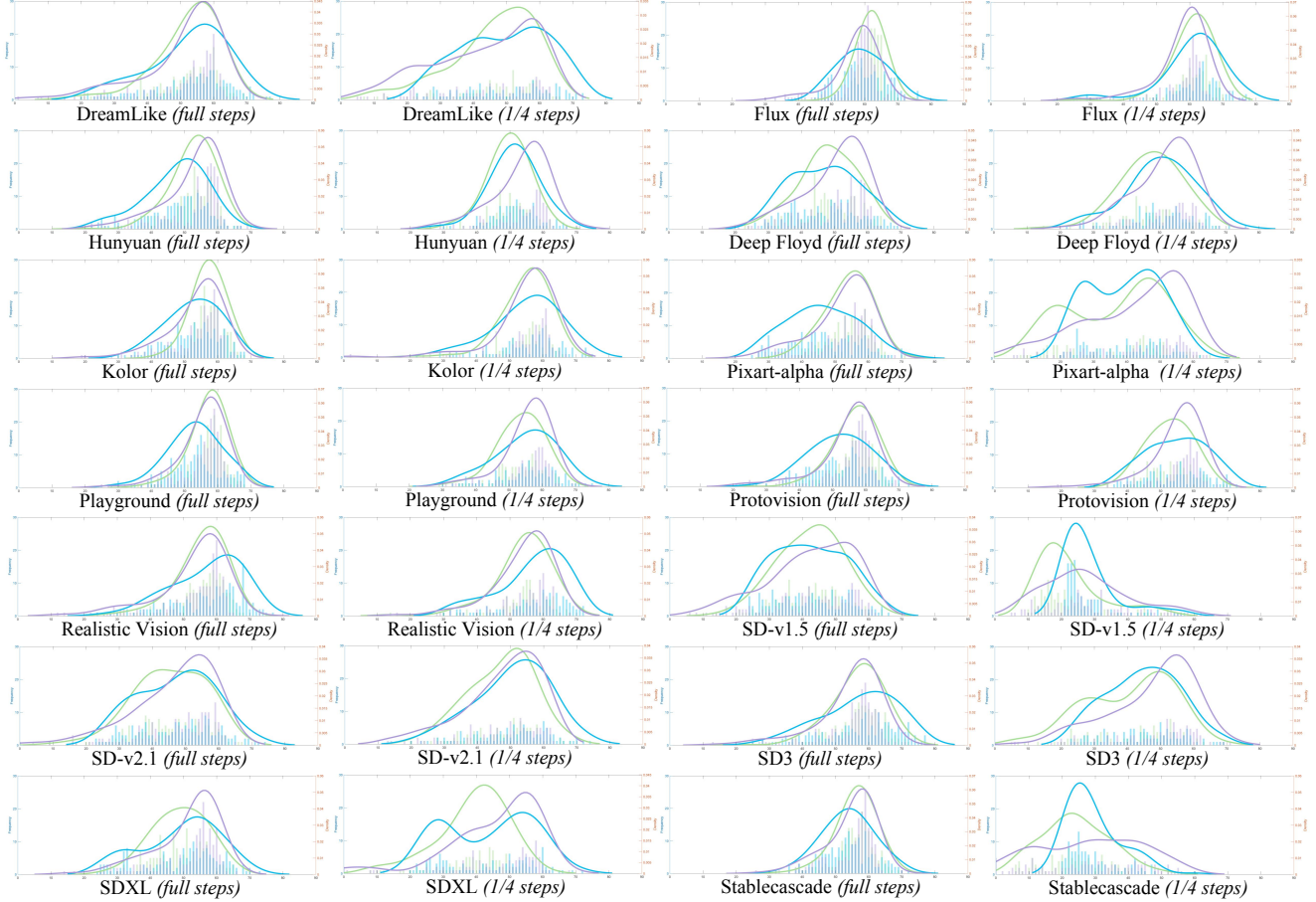


Figure 13. **MOS distribution histograms and kernel density curves across different face generation models.** “full steps” contains images generated in default sampling steps and “1/4 steps” contains the images generated by one-quarter of the default steps.

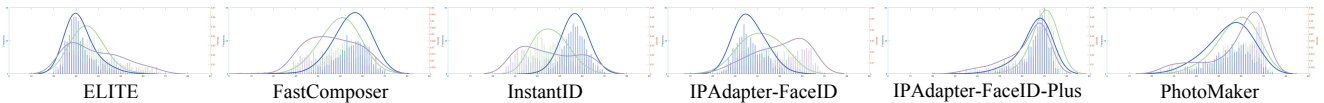


Figure 14. **MOS distribution histograms and kernel density curves across different face customization models.**

tently across all evaluation dimensions, with minimal variability observed. However, when it comes to face restoration tasks, the *quality* and *identity fidelity* of the male class are better. This suggests that generation and customization models trained on extensive datasets exhibit less gender bias than restoration models trained on smaller datasets.

## D. QA Methods Implementation Details

**Evaluation Metrics** We adopt three widely used metrics in IQA [82, 83]: Spearman rank-order correlation coefficient (SRCC), Pearson linear correlation coefficient (PLCC), and Kendall rank correlation coefficient (KLCC) to evaluate the performance of quality assessment methods.

**SRCC**, which ranges from -1 to 1, evaluates the mono-

tonic relationship between two variables. For  $N$  images, it is computed as:

$$SRCC = 1 - \frac{6 \sum_{n=1}^N (v_n - p_n)^2}{N(N^2 - 1)}, \quad (8)$$

Here,  $v_n$  represents the rank of the ground truth value  $y_n$ , while  $p_n$  corresponds to the rank of the predicted value  $\hat{y}_n$ . When the SRCC value is higher, it signifies a stronger monotonic agreement between the ground truth and the predicted scores. **PLCC** quantifies the linear correlation between predicted scores and ground truth scores and is for-



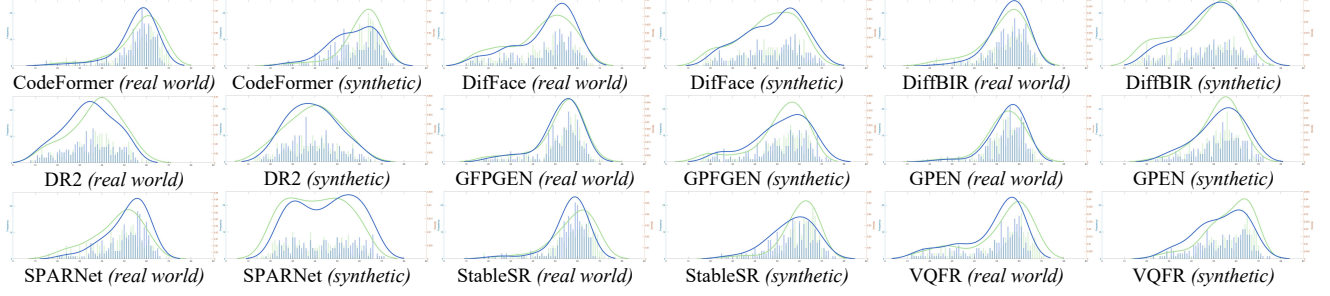


Figure 15. **MOS distribution histograms and kernel density curves across different face restoration models.** “synthetic” refers to images restored from the synthetic low-quality inputs while “real world” refers to the images restored from real-world low-quality inputs.

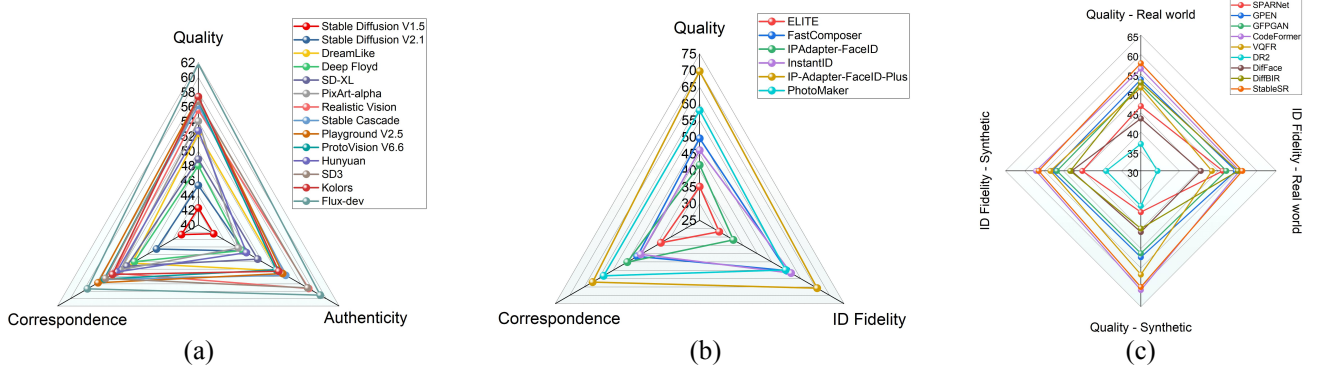


Figure 16. **Comparison of averaged MOS of different models across Quality, Authenticity, ID Fidelity, and Correspondence.** (a) Face generation models. (b) Face customization models. (c) Face restoration models.

culated as:

$$PLCC = \frac{\sum_{n=1}^N (y_n - \bar{y})(\hat{y}_n - \bar{\hat{y}})}{\sqrt{\sum_{n=1}^N (y_n - \bar{y})^2} \sqrt{\sum_{n=1}^N (\hat{y}_n - \bar{\hat{y}})^2}}, \quad (9)$$

where  $\bar{y}$  and  $\bar{\hat{y}}$  denote the mean values of the ground truth scores and the predicted scores, respectively. **KLCC** measures the ordinal association between two measured quantities and is defined as:

$$KLCC = \frac{2(C - D)}{N(N - 1)}, \quad (10)$$

where  $C$  is the number of concordant pairs and  $D$  is the number of discordant pairs among all possible pairs of  $N$  data points. A higher KLCC indicates a stronger rank correlation between the two variables. Together, these metrics provide a comprehensive evaluation of the relationship between predicted preference scores and ground truth MOS values across different aspects of correlation.

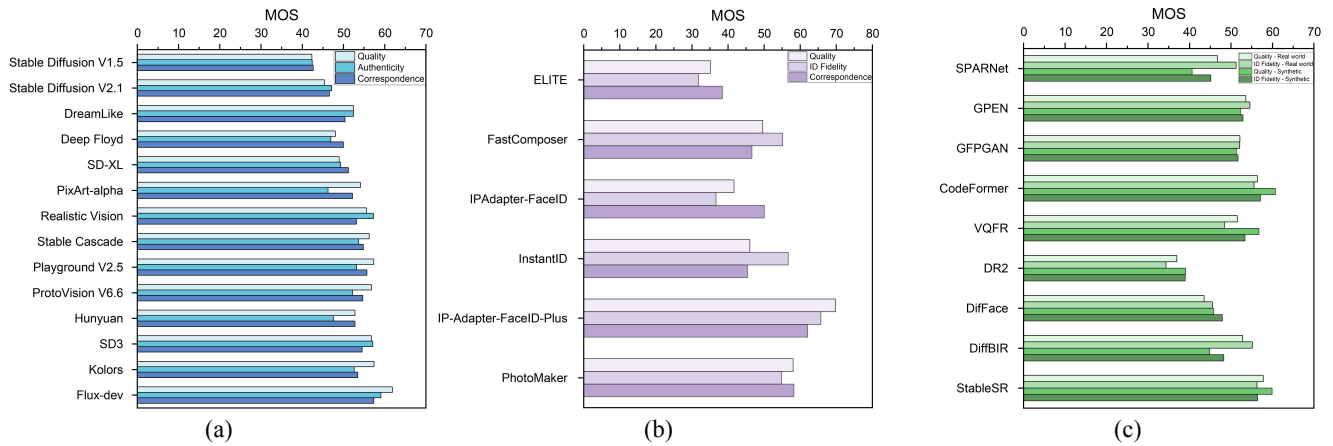


Figure 17. **Comparison of different model rankings based on the averaged MOS** (a) Face generation models. (b) Face customization models. (c) Face restoration models.

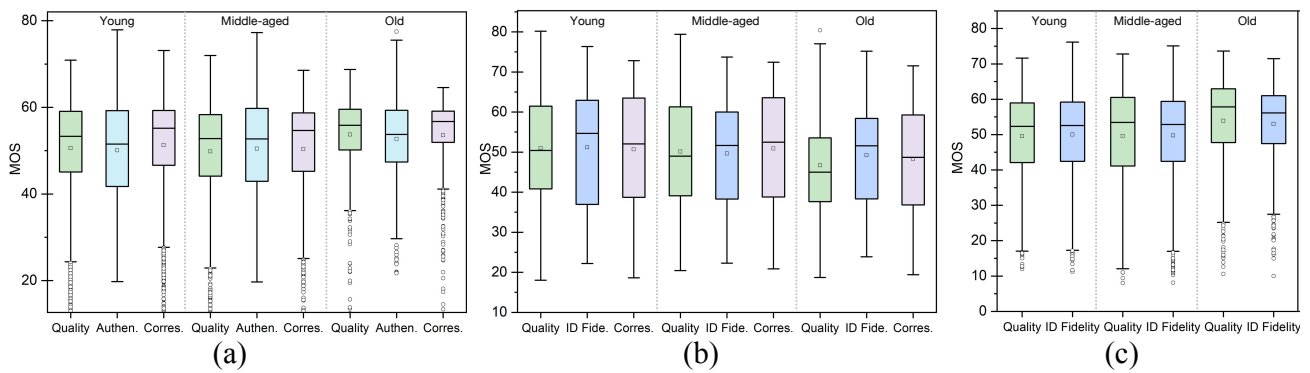


Figure 18. **Comparison of multi-dimensional MOS distributions across age groups.** “Authen.”, “Corres.” and “ID Fide.” denote *Authenticity*, *Correspondence*, and *ID Fidelity* respectively. (a) Face generation models. (b) Face customization models. (c) Face restoration models.

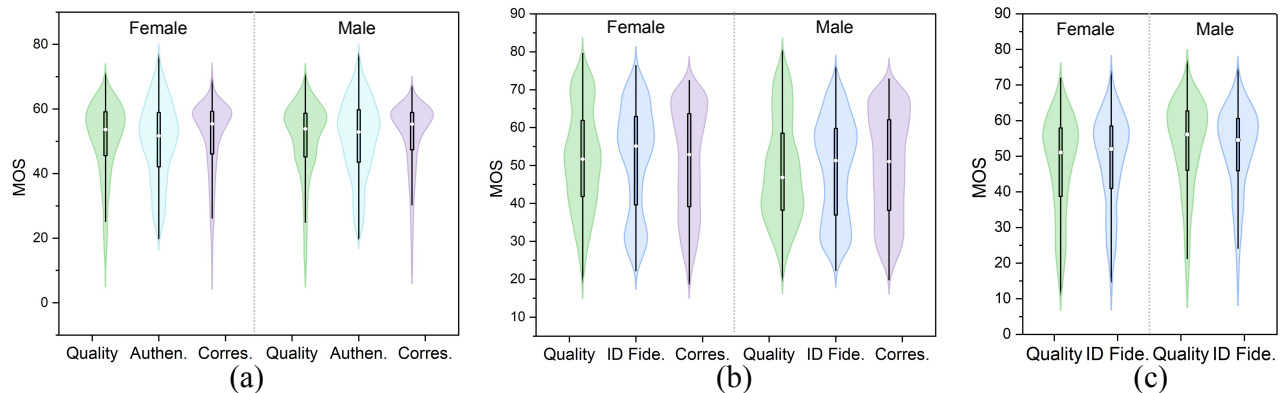


Figure 19. **Comparison of multi-dimensional MOS distributions across genders.** “Authen.”, “Corres.” and “ID Fide.” denote *Authenticity*, *Correspondence*, and *ID Fidelity* respectively. (a) Face generation models. (b) Face customization models. (c) Face restoration models.

## References

- [1] Lacey Best-Rowden and Anil K Jain. Learning face image quality from human assessments. *IEEE Transactions on Information forensics and security*, 13(12):3064–3077, 2018. 2, 3
- [2] Fadi Boutros, Meiling Fang, Marcel Klemm, Biying Fu, and Naser Damer. Cr-fiq: face image quality assessment by learning sample relative classifiability. In *Proceedings of the IEEE/CVF Conference on Computer Vision and Pattern Recognition*, pages 5836–5845, 2023. 3
- [3] Nicolas Chahine, Ana-Stefania Calarasanu, Davide Garcia-Civiero, Theo Cayla, Sira Ferradans, and Jean Ponce. An image quality assessment dataset for portraits, 2023. 2, 3
- [4] Chaofeng Chen, Dihong Gong, Hao Wang, Zhifeng Li, and Kwan-Yee K Wong. Learning spatial attention for face super-resolution. *IEEE Transactions on Image Processing*, 30:1219–1231, 2020. 2, 4, 7, 9, 12
- [5] Chaofeng Chen, Xiaoming Li, Lingbo Yang, Xianhui Lin, Lei Zhang, and Kwan-Yee K Wong. Progressive semantic-aware style transformation for blind face restoration. In *Proceedings of the IEEE/CVF Conference on Computer Vision and Pattern Recognition*, pages 11896–11905, 2021. 2
- [6] Junsong Chen, Jincheng Yu, Chongjian Ge, Lewei Yao, Enze Xie, Yue Wu, Zhongdao Wang, James Kwok, Ping Luo, Huchuan Lu, and Zhenguo Li. Pixart- $\alpha$ : Fast training of diffusion transformer for photorealistic text-to-image synthesis, 2023. 2, 3, 9, 12
- [7] Wei-Ting Chen, Gurunandan Krishnan, Qiang Gao, Sy-Yen Kuo, Sizhuo Ma, and Jian Wang. Dsl-fiq: Assessing facial image quality via dual-set degradation learning and landmark-guided transformer, 2024. 2, 3
- [8] Wei-Ting Chen, Gurunandan Krishnan, Qiang Gao, Sy-Yen Kuo, Sizhou Ma, and Jian Wang. Dsl-fiq: Assessing facial image quality via dual-set degradation learning and landmark-guided transformer. In *Proceedings of the IEEE/CVF Conference on Computer Vision and Pattern Recognition*, pages 2931–2941, 2024. 7, 8
- [9] Yu Chen, Ying Tai, Xiaoming Liu, Chunhua Shen, and Jian Yang. Fsrnet: End-to-end learning face super-resolution with facial priors. In *Proceedings of the IEEE Conference on Computer Vision and Pattern Recognition*, pages 2492–2501, 2018. 2
- [10] Siying Cui, Jiankang Deng, Jia Guo, Xiang An, Yongle Zhao, Xinyu Wei, and Ziyong Feng. Idadapter: Learning mixed features for tuning-free personalization of text-to-image models. *arXiv preprint arXiv:2403.13535*, 2024. 2
- [11] Deep Floyd Contributors. Deep Floyd. Available: <https://github.com/deep-floyd/IF>. Accessed: 2024-10-03. 2, 3, 9
- [12] Jiankang Deng, Jia Guo, Niannan Xue, and Stefanos Zafeiriou. Arcface: Additive angular margin loss for deep face recognition. In *Proceedings of the IEEE/CVF conference on computer vision and pattern recognition*, pages 4690–4699, 2019. 7, 8
- [13] Dreamlike V2 Contributors. Dreamlike V2. Available: <https://huggingface.co/dreamlike-art/dreamlike-photoreal-2.0>. Accessed: 2024-10-03. 6, 9
- [14] Flux-dev Contributors. Flux-dev. Available: <https://huggingface.co/black-forest-labs/FLUX.1-dev>. Accessed: 2024-10-03. 3, 6, 9, 12, 13
- [15] Rinon Gal, Yuval Alaluf, Yuval Atzmon, Or Patashnik, Amit H Bermano, Gal Chechik, and Daniel Cohen-Or. An image is worth one word: Personalizing text-to-image generation using textual inversion. *arXiv preprint arXiv:2208.01618*, 2022. 2
- [16] S. Alireza Golestaneh, Saba Dadsetan, and Kris M. Kitani. No-reference image quality assessment via transformers, relative ranking, and self-consistency. In *Proceedings of the IEEE/CVF Winter Conference on Applications of Computer Vision (WACV)*, pages 1220–1230, 2022. 7, 8
- [17] Ian J. Goodfellow, Jean Pouget-Abadie, Mehdi Mirza, Bing Xu, David Warde-Farley, Sherjil Ozair, Aaron Courville, and Yoshua Bengio. Generative adversarial networks, 2014. 2
- [18] GPT-4o Contributors. GPT-4o. Available: <https://chatgpt.com/>. Accessed: 2024-10-10. 3
- [19] Ke Gu, Guangtao Zhai, Min Liu, Xiaokang Yang, Wenjun Zhang, Xianghui Sun, Wanhong Chen, and Ying Zuo. Fisblim: A five-step blind metric for quality assessment of multiply distorted images. In *Proceedings of the SiPS*, pages 241–246, 2013. 7, 8
- [20] Yuchao Gu, Xintao Wang, Liangbin Xie, Chao Dong, Gen Li, Ying Shan, and Ming-Ming Cheng. Vqfr: Blind face restoration with vector-quantized dictionary and parallel decoder. *arXiv preprint arXiv:2205.06803*, 2022. 2, 4, 9
- [21] Kaiming He, Xiangyu Zhang, Shaoqing Ren, and Jian Sun. Deep residual learning for image recognition. In *2016 IEEE Conference on Computer Vision and Pattern Recognition (CVPR)*, pages 770–778, 2016. 7, 8
- [22] Xuanhua He, Quande Liu, Shengju Qian, Xin Wang, Tao Hu, Ke Cao, Keyu Yan, Man Zhou, and Jie Zhang. Id-animator: Zero-shot identity-preserving human video generation. *arXiv preprint arXiv:2404.15275*, 2024. 2
- [23] Javier Hernandez-Ortega, Javier Galbally, Julian Fierrez, Rudolf Haraksim, and Laurent Beslay. Faceqnet: Quality assessment for face recognition based on deep learning. In *2019 International Conference on Biometrics (ICB)*, pages 1–8. IEEE, 2019. 3
- [24] Jack Hessel, Ari Holtzman, Maxwell Forbes, Ronan Le Bras, and Yejin Choi. CLIPScore: A Reference-free Evaluation Metric for Image Captioning. *arXiv e-prints*, art. arXiv:2104.08718, 2021. 7, 8
- [25] Jonathan Ho, Ajay Jain, and Pieter Abbeel. Denoising diffusion probabilistic models. *Advances in neural information processing systems*, 33:6840–6851, 2020. 2
- [26] Alain Hore and Djemel Ziou. Image quality metrics: Psnr vs. ssim. In *2010 20th international conference on pattern recognition*, pages 2366–2369. IEEE, 2010. 7, 8
- [27] Gary B. Huang, Manu Ramesh, Tamara Berg, and Erik Learned-Miller. Labeled faces in the wild: A database

- for studying face recognition in unconstrained environments. Technical Report 07-49, University of Massachusetts, Amherst, 2007. 4
- [28] IP-Adapter-FaceID-Plus Contributors. IP-Adapter-FaceID-Plus. Available: <https://huggingface.co/h94/IP-Adapter-FaceID>. Accessed: 2024-10-03. 3, 6, 9, 13
- [29] IP-Adapter-FaceID-SDXL Contributors. IP-Adapter-FaceID-SDXL. Available: <https://huggingface.co/h94/IP-Adapter>. Accessed: 2024-10-03. 3, 6, 9
- [30] Le Kang, Peng Ye, Yi Li, and David Doermann. Convolutional neural networks for no-reference image quality assessment. In *Proceedings of the IEEE Conference on Computer Vision and Pattern Recognition (CVPR)*, 2014. 7, 8
- [31] Tero Karras, Samuli Laine, and Timo Aila. A style-based generator architecture for generative adversarial networks, 2019. 2
- [32] Ira Kemelmacher-Shlizerman, Steven M Seitz, Daniel Miller, and Evan Brossard. The megaface benchmark: 1 million faces for recognition at scale. In *Proceedings of the IEEE conference on computer vision and pattern recognition*, pages 4873–4882, 2016. 4
- [33] Deokyun Kim, Minseon Kim, Gihyun Kwon, and Dae-Shik Kim. Progressive face super-resolution via attention to facial landmark. *arXiv preprint arXiv:1908.08239*, 2019. 2
- [34] Diederik P Kingma and Max Welling. Auto-encoding variational bayes, 2022. 2
- [35] Yuval Kirstain, Adam Polyak, Uriel Singer, Shahbuland Matiana, Joe Penna, and Omer Levy. Pick-a-pic: An open dataset of user preferences for text-to-image generation, 2023. 2, 3
- [36] Kolors Contributors. Kolors. Available: <https://huggingface.co/Kwai-Kolors/Kolors>. Accessed: 2024-10-03. 3, 9, 13
- [37] Nupur Kumari, Bingliang Zhang, Richard Zhang, Eli Shechtman, and Jun-Yan Zhu. Multi-concept customization of text-to-image diffusion, 2023. 2
- [38] Chunyi Li, Zicheng Zhang, Haoning Wu, Wei Sun, Xiongkuo Min, Xiaohong Liu, Guangtao Zhai, and Weisi Lin. Aqiqa-3k: An open database for ai-generated image quality assessment, 2023. 2, 3
- [39] Daiqing Li, Aleks Kamko, Ehsan Akhgari, Ali Sabet, Linmiao Xu, and Suhail Doshi. Playground v2.5: Three insights towards enhancing aesthetic quality in text-to-image generation, 2024. 3, 9, 12
- [40] Junnan Li, Dongxu Li, Caiming Xiong, and Steven Hoi. Blip: Bootstrapping language-image pre-training for unified vision-language understanding and generation. In *International conference on machine learning*, pages 12888–12900. PMLR, 2022. 7, 8
- [41] Xiaoming Li, Ming Liu, Yuting Ye, Wangmeng Zuo, Liang Lin, and Ruigang Yang. Learning warped guidance for blind face restoration. In *The European Conference on Computer Vision (ECCV)*, 2018. 2
- [42] Xiaoming Li, Wenyu Li, Dongwei Ren, Hongzhi Zhang, Meng Wang, and Wangmeng Zuo. Enhanced blind face restoration with multi-exemplar images and adaptive spatial feature fusion. In *Proceedings of the IEEE/CVF Conference on Computer Vision and Pattern Recognition*, pages 2706–2715, 2020. 2
- [43] Xiaoming Li, Shiguang Zhang, Shangchen Zhou, Lei Zhang, and Wangmeng Zuo. Learning dual memory dictionaries for blind face restoration. *IEEE Transactions on Pattern Analysis and Machine Intelligence*, 2022. 4
- [44] Zhen Li, Mingdeng Cao, Xintao Wang, Zhongang Qi, Ming-Ming Cheng, and Ying Shan. Photomaker: Customizing realistic human photos via stacked id embedding. *arXiv preprint arXiv:2312.04461*, 2023. 2, 3, 6, 9
- [45] Zhimin Li, Jianwei Zhang, Qin Lin, Jiangfeng Xiong, Yanxin Long, Xincheng Deng, Yingfang Zhang, Xingchao Liu, Minbin Huang, Zedong Xiao, Dayou Chen, Jiajun He, Jiahao Li, Wenyue Li, Chen Zhang, Rongwei Quan, Jianxiang Lu, Jiabin Huang, Xiaoyan Yuan, Xiaoxiao Zheng, Yixuan Li, Jihong Zhang, Chao Zhang, Meng Chen, Jie Liu, Zheng Fang, Weiyan Wang, Jinbao Xue, Yangyu Tao, Jianchen Zhu, Kai Liu, Sihuan Lin, Yifu Sun, Yun Li, Dongdong Wang, Mingtao Chen, Zhichao Hu, Xiao Xiao, Yan Chen, Yuhong Liu, Wei Liu, Di Wang, Yong Yang, Jie Jiang, and Qinglin Lu. Hunyuan-dit: A powerful multi-resolution diffusion transformer with fine-grained chinese understanding, 2024. 2, 3, 6, 9
- [46] Youwei Liang, Junfeng He, Gang Li, Peizhao Li, Arseniy Klimovskiy, Nicholas Carolan, Jiao Sun, Jordi Pont-Tuset, Sarah Young, Feng Yang, et al. Rich human feedback for text-to-image generation. In *Proceedings of the IEEE/CVF Conference on Computer Vision and Pattern Recognition*, pages 19401–19411, 2024. 2, 3
- [47] Zhang Lijun, Shao Xiaohu, Yang Fei, Deng Pingling, Zhou Xiangdong, and Shi Yu. Multi-branch face quality assessment for face recognition. In *2019 IEEE 19th International Conference on Communication Technology (ICCT)*, pages 1659–1664. IEEE, 2019. 3
- [48] Tsung-Yi Lin, Michael Maire, Serge J. Belongie, Lubomir D. Bourdev, Ross B. Girshick, James Hays, Pietro Perona, Deva Ramanan, Piotr Dollár, and C. Lawrence Zitnick. Microsoft COCO: common objects in context. *CoRR*, abs/1405.0312, 2014. 3
- [49] Xinqi Lin, Jingwen He, Ziyang Chen, Zhaoyang Lyu, Ben Fei, Bo Dai, Wanli Ouyang, Yu Qiao, and Chao Dong. Diffbir: Towards blind image restoration with generative diffusion prior. *arXiv preprint arXiv:2308.15070*, 2023. 2, 4, 7, 9
- [50] Tie Liu, Shengxi Li, Mai Xu, Li Yang, and Xiaofei Wang. Assessing face image quality: A large-scale database and a transformer method. *IEEE Transactions on Pattern Analysis and Machine Intelligence*, 46(5):3981–4000, 2024. 2, 3
- [51] Ziwei Liu, Ping Luo, Xiaogang Wang, and Xiaoou Tang. Deep learning face attributes in the wild. In *Proceedings of International Conference on Computer Vision (ICCV)*, 2015. 4
- [52] Xiongkuo Min, Ke Gu, Guangtao Zhai, Jing Liu, Xiaokang Yang, and Chang Wen Chen. Blind quality assessment based on pseudo-reference image. *IEEE Transactions on Multimedia*, 20(8):2049–2062, 2018. 7, 8

- [53] Xionghuo Min, Guangtao Zhai, Ke Gu, Yutao Liu, and Xiaokang Yang. Blind image quality estimation via distortion aggravation. *IEEE Transactions on Broadcasting*, 64(2): 508–517, 2018. 8
- [54] Anish Mittal, Rajiv Soundararajan, and Alan C. Bovik. Making a “completely blind” image quality analyzer. *IEEE Signal Processing Letters*, 20(3):209–212, 2013. 7, 8
- [55] Stylianos Moschoglou, Athanasios Papaioannou, Christos Sagonas, Jiankang Deng, Irene Kotsia, and Stefanos Zafeiriou. Agedb: the first manually collected, in-the-wild age database. In *proceedings of the IEEE conference on computer vision and pattern recognition workshops*, pages 51–59, 2017. 4
- [56] Fu-Zhao Ou, Xingyu Chen, Ruixin Zhang, Yuge Huang, Shaoxin Li, Jilin Li, Yong Li, Liujuan Cao, and Yuan-Gen Wang. Sdd-fiq: Unsupervised face image quality assessment with similarity distribution distance. In *Proceedings of the IEEE/CVF conference on computer vision and pattern recognition*, pages 7670–7679, 2021. 2, 3
- [57] William Peebles and Saining Xie. Scalable diffusion models with transformers, 2023. 2
- [58] Pablo Pernias, Dominic Rampas, Mats L Richter, Christopher J Pal, and Marc Aubreville. Würstchen: An efficient architecture for large-scale text-to-image diffusion models. *arXiv preprint arXiv:2306.00637*, 2023. 3, 9, 12
- [59] Dustin Podell, Zion English, Kyle Lacey, Andreas Blattmann, Tim Dockhorn, Jonas Müller, Joe Penna, and Robin Rombach. Sdxl: Improving latent diffusion models for high-resolution image synthesis, 2023. 2, 3, 6, 9, 12
- [60] ProtoVision V6.6 Contributors. ProtoVision V6.6. Available: <https://huggingface.co/stablediffusionapi/protovision-xl-v6.6/tree/41d371a64dbf0e498e51073ed2a2fab46fa3f985>. Accessed: 2024-10-03. 3, 9
- [61] Lu Qi, Jason Kuen, Yi Wang, Jiuxiang Gu, Hengshuang Zhao, Philip Torr, Zhe Lin, and Jiaya Jia. Open world entity segmentation. *IEEE Transactions on Pattern Analysis and Machine Intelligence*, 45(7):8743–8756, 2022. 3
- [62] Aditya Ramesh, Mikhail Pavlov, Gabriel Goh, Scott Gray, Chelsea Voss, Alec Radford, Mark Chen, and Ilya Sutskever. Zero-shot text-to-image generation, 2021. 2
- [63] Aditya Ramesh, Prafulla Dhariwal, Alex Nichol, Casey Chu, and Mark Chen. Hierarchical text-conditional image generation with clip latents. *arXiv preprint arXiv:2204.06125*, 2022. 2
- [64] Aditya Ramesh, Prafulla Dhariwal, Alex Nichol, Casey Chu, and Mark Chen. Hierarchical text-conditional image generation with clip latents, 2022. 2
- [65] Realistic Vision V5.1 Contributors. Realistic Vision V5.1. Available: [https://huggingface.co/SG161222/Realistic\\_Vision\\_V5.1\\_noVAE](https://huggingface.co/SG161222/Realistic_Vision_V5.1_noVAE). Accessed: 2024-10-03. 3, 6, 9, 12
- [66] Robin Rombach, Andreas Blattmann, Dominik Lorenz, Patrick Esser, and Björn Ommer. High-resolution image synthesis with latent diffusion models. In *Proceedings of the IEEE/CVF Conference on Computer Vision and Pattern Recognition (CVPR)*, pages 10684–10695, 2022. 2
- [67] Robin Rombach, Andreas Blattmann, Dominik Lorenz, Patrick Esser, and Björn Ommer. High-resolution image synthesis with latent diffusion models. In *Proceedings of the IEEE/CVF conference on computer vision and pattern recognition*, pages 10684–10695, 2022. 3, 13
- [68] Robin Rombach, Andreas Blattmann, Dominik Lorenz, Patrick Esser, and Björn Ommer. High-resolution image synthesis with latent diffusion models, 2022. 2, 9
- [69] Nataniel Ruiz, Yuanzhen Li, Varun Jampani, Yael Pritch, Michael Rubinstein, and Kfir Aberman. Dreambooth: Fine tuning text-to-image diffusion models for subject-driven generation. In *Proceedings of the IEEE/CVF Conference on Computer Vision and Pattern Recognition*, pages 22500–22510, 2023. 2
- [70] Chitwan Saharia, William Chan, Saurabh Saxena, Lala Li, Jay Whang, Emily Denton, Seyed Kamyar Seyed Ghasemipour, Burcu Karagol Ayan, S. Sara Mahdavi, Rapha Gontijo Lopes, Tim Salimans, Jonathan Ho, David J Fleet, and Mohammad Norouzi. Photorealistic text-to-image diffusion models with deep language understanding, 2022. 2
- [71] Chitwan Saharia, William Chan, Saurabh Saxena, Lala Li, Jay Whang, Emily L Denton, Kamyar Ghasemipour, Raphael Gontijo Lopes, Burcu Karagol Ayan, Tim Salimans, et al. Photorealistic text-to-image diffusion models with deep language understanding. *Advances in Neural Information Processing Systems*, 35:36479–36494, 2022. 2
- [72] SD3 Contributors. SD3. Available: <https://huggingface.co/stabilityai/stable-diffusion-3-medium>. Accessed: 2024-10-03. 3, 6, 9, 12, 13
- [73] B Series. Methodology for the subjective assessment of the quality of television pictures. *Recommendation ITU-R BT, 500(13)*, 2012. 5
- [74] Qi Shan, Brian Curless, Yasutaka Furukawa, Carlos Hernandez, and Steven M Seitz. Photo uncrop. In *Computer Vision—ECCV 2014: 13th European Conference, Zurich, Switzerland, September 6–12, 2014, Proceedings, Part VI 13*, pages 16–31. Springer, 2014. 13
- [75] M Six Silberman, Bill Tomlinson, Rochelle LaPlante, Joel Ross, Lilly Irani, and Andrew Zaldivar. Responsible research with crowds: pay crowdworkers at least minimum wage. *Communications of the ACM*, 61(3):39–41, 2018. 10
- [76] Karen Simonyan and Andrew Zisserman. Very Deep Convolutional Networks for Large-Scale Image Recognition. *arXiv e-prints*, art. arXiv:1409.1556, 2014. 7, 8
- [77] Jiaming Song, Chenlin Meng, and Stefano Ermon. Denoising diffusion implicit models. *arXiv:2010.02502*, 2020. 2
- [78] Shaolin Su, Qingsen Yan, Yu Zhu, Cheng Zhang, Xin Ge, Jinqiu Sun, and Yanning Zhang. Blindly assess image quality in the wild guided by a self-adaptive hyper network. In *2020 IEEE/CVF Conference on Computer Vision and Pattern Recognition (CVPR)*, pages 3664–3673, 2020. 7, 8
- [79] Shaolin Su, Hanhe Lin, Vlad Hosu, Oliver Wiedemann, Jinqiu Sun, Yu Zhu, Hantao Liu, Yanning Zhang, and Dietmar Saupe. Going the extra mile in face image quality assessment: A novel database and model, 2023. 2, 3

- [80] Philipp Terhorst, Jan Niklas Kolf, Naser Damer, Florian Kirchbuchner, and Arjan Kuijper. Ser-fiq: Unsupervised estimation of face image quality based on stochastic embedding robustness. In *Proceedings of the IEEE/CVF conference on computer vision and pattern recognition*, pages 5651–5660, 2020. 7, 8
- [81] Yuri Viazovetskiy, Vladimir Ivashkin, and Evgeny Kashin. Stylegan2 distillation for feed-forward image manipulation. In *Computer Vision–ECCV 2020: 16th European Conference, Glasgow, UK, August 23–28, 2020, Proceedings, Part XXII 16*, pages 170–186. Springer, 2020. 2
- [82] Jiarui Wang, Huiyu Duan, Jing Liu, Shi Chen, Xiongkuo Min, and Guangtao Zhai. Aigciqa2023: A large-scale image quality assessment database for ai generated images: from the perspectives of quality, authenticity and correspondence. In *Proceedings of the CAAI International Conference on Artificial Intelligence (CICAI)*, pages 46–57. Springer, 2023. 16
- [83] Jiarui Wang, Huiyu Duan, Jing Liu, Shi Chen, Xiongkuo Min, and Guangtao Zhai. Aigciqa2023: A large-scale image quality assessment database for ai generated images: from the perspectives of quality, authenticity and correspondence, 2023. 2, 3, 16
- [84] Jianyi Wang, Zongsheng Yue, Shangchen Zhou, Kelvin CK Chan, and Chen Change Loy. Exploiting diffusion prior for real-world image super-resolution. *arXiv preprint arXiv:2305.07015*, 2023. 2, 4
- [85] Jiarui Wang, Huiyu Duan, Guangtao Zhai, and Xiongkuo Min. Understanding and evaluating human preferences for ai generated images with instruction tuning. *arXiv preprint arXiv:2405.07346*, 2024. 7, 8
- [86] Jianyi Wang, Zongsheng Yue, Shangchen Zhou, Kelvin C. K. Chan, and Chen Change Loy. Exploiting diffusion prior for real-world image super-resolution, 2024. 6, 7, 9
- [87] Liangbin Xie, Xintao Wang, Honglun Zhang, Chao Dong, and Ying Shan. Vfhq: A high-quality dataset and benchmark for video face super-resolution, 2022. 4
- [88] Qixun Wang, Xu Bai, Haofan Wang, Zekui Qin, and Anthony Chen. Instantid: Zero-shot identity-preserving generation in seconds. *arXiv preprint arXiv:2401.07519*, 2024. 2, 3, 6, 9, 13
- [89] Tao Wang, Kaihao Zhang, Xuanxi Chen, Wenhan Luo, Jiankang Deng, Tong Lu, Xiaochun Cao, Wei Liu, Hongdong Li, and Stefanos Zafeiriou. A survey of deep face restoration: Denoise, super-resolution, deblur, artifact removal, 2022. 2
- [90] Xintao Wang, Liangbin Xie, Chao Dong, and Ying Shan. Real-esrgan: Training real-world blind super-resolution with pure synthetic data. In *International Conference on Computer Vision Workshops (ICCVW)*. 4, 10
- [91] Xintao Wang, Yu Li, Honglun Zhang, and Ying Shan. Towards real-world blind face restoration with generative facial prior. In *The IEEE Conference on Computer Vision and Pattern Recognition (CVPR)*, 2021. 2, 4, 7, 9
- [92] Xintao Wang, Yu Li, Honglun Zhang, and Ying Shan. Towards real-world blind face restoration with generative facial prior. In *CVPR*, 2021. 4, 9
- [93] Zhou Wang, Alan C Bovik, Hamid R Sheikh, and Eero P Simoncelli. Image quality assessment: from error visibility to structural similarity. *IEEE transactions on image processing*, 13(4):600–612, 2004. 7, 8
- [94] Zhixin Wang, Ziyang Zhang, Xiaoyun Zhang, Huangjie Zheng, Mingyuan Zhou, Ya Zhang, and Yanfeng Wang. Dr2: Diffusion-based robust degradation remover for blind face restoration. In *Proceedings of the IEEE/CVF Conference on Computer Vision and Pattern Recognition*, pages 1704–1713, 2023. 2, 4, 6, 9
- [95] Yuxiang Wei, Yabo Zhang, Zhilong Ji, Jinfeng Bai, Lei Zhang, and Wangmeng Zuo. Elite: Encoding visual concepts into textual embeddings for customized text-to-image generation, 2023. 2, 3, 6, 9
- [96] Xiaoshi Wu, Keqiang Sun, Feng Zhu, Rui Zhao, and Hongsheng Li. Human preference score: Better aligning text-to-image models with human preference, 2023. 2, 3
- [97] Guangxuan Xiao, Tianwei Yin, William T. Freeman, Frédo Durand, and Song Han. Fastcomposer: Tuning-free multi-subject image generation with localized attention, 2023. 2, 3, 6, 9
- [98] Jingtao Xu, Peng Ye, Qiaohong Li, Haiqing Du, Yong Liu, and David S. Doermann. Blind image quality assessment based on high order statistics aggregation. *IEEE Transactions on Image Processing*, 25:4444–4457, 2016. 7, 8
- [99] Jiazheng Xu, Xiao Liu, Yuchen Wu, Yuxuan Tong, Qinkai Li, Ming Ding, Jie Tang, and Yuxiao Dong. Imagereward: Learning and evaluating human preferences for text-to-image generation. *Advances in Neural Information Processing Systems*, 36, 2024. 7
- [100] Shuo Yang, Ping Luo, Chen-Change Loy, and Xiaoou Tang. Wider face: A face detection benchmark. In *Proceedings of the IEEE conference on computer vision and pattern recognition*, pages 5525–5533, 2016. 4
- [101] Sidi Yang, Tianhe Wu, Shuwei Shi, Shanshan Lao, Yuan Gong, Mingdeng Cao, Jiahao Wang, and Yujiu Yang. MANIQA: Multi-dimension Attention Network for No-Reference Image Quality Assessment. *arXiv e-prints*, art. arXiv:2204.08958, 2022. 7, 8
- [102] Tao Yang, Peiran Ren, Xuansong Xie, and Lei Zhang. Gan prior embedded network for blind face restoration in the wild. In *Proceedings of the IEEE/CVF Conference on Computer Vision and Pattern Recognition*, pages 672–681, 2021. 2, 4, 9
- [103] Hu Ye, Jun Zhang, Sibio Liu, Xiao Han, and Wei Yang. Ip-adapt: Text compatible image prompt adapter for text-to-image diffusion models. *arXiv preprint arXiv:2308.06721*, 2023. 2
- [104] Zongsheng Yue and Chen Change Loy. Difface: Blind face restoration with diffused error contraction. *arXiv preprint arXiv:2212.06512*, 2022. 2, 4, 9
- [105] Lin Zhang, Lei Zhang, and Alan C. Bovik. A feature-enriched completely blind image quality evaluator. *IEEE Transactions on Image Processing*, 24(8):2579–2591, 2015. 7, 8
- [106] Richard Zhang, Phillip Isola, Alexei A Efros, Eli Shechtman, and Oliver Wang. The unreasonable effectiveness of

deep features as a perceptual metric. In *Proceedings of the IEEE conference on computer vision and pattern recognition*, pages 586–595, 2018. [7](#), [8](#)

- [107] Shangchen Zhou, Kelvin Chan, Chongyi Li, and Chen Change Loy. Towards robust blind face restoration with codebook lookup transformer. *Advances in Neural Information Processing Systems*, 35:30599–30611, 2022. [2](#), [4](#), [6](#), [9](#), [13](#)